Condensates from vapor made by impacts between metal-, silicate-rich bodies: Comparison with metal and chondrules in CB chondrites

Alexei V. Fedkin[1], Lawrence Grossman[1,2], Munir Humayun[3], Steven B. Simon[1] and Andrew J. Campbell[1]

[1]Dept. of the Geophysical Sciences,
The University of Chicago,
5734 South Ellis Avenue,
Chicago, Illinois 60637.

[3]National High Magnetic Field Laboratory and
Dept. of Earth, Ocean and Atmospheric Science,
Florida State University,
Tallahassee, Florida 32310.

Submitted to *Geochimica et Cosmochimica Acta*,

January 15, 2015.

Revised version submitted May , 2015.

[2]Also Enrico Fermi Institute, The University of Chicago.

ABSTRACT

The impact hypothesis for the origin of CB chondrites was tested by performing equilibrium condensation calculations in systems composed of vaporized mixtures of projectile and target materials. When one of the impacting bodies is composed of the metal from CR chondrites and the other is an H chondrite, good agreement can be found between calculated and observed compositions of unzoned metal grains in CB chondrites but the path of composition variation of the silicate condensate computed for the same conditions that reproduce the metal grain compositions does not pass through the measured compositions of barred olivine (BO) or cryptocrystalline (CC) chondrules in the CBs. The discrepancy between measured chondrule compositions and those of calculated silicates is not reduced when diogenite, eucrite or howardite compositions are substituted for H chondrite as the silicate-rich impacting body. If, however, a CR chondrite body is differentiated into core, a relatively CaO-, Al_2O_3-poor mantle and a CaO-, Al_2O_3-rich crust, and later accretes significant amounts of water, a collision between it and an identical body can produce the necessary chemical conditions for condensation of CB chondrules. If the resulting impact plume is spatially heterogeneous in its proportions of crust and mantle components, the composition paths calculated for silicate condensates at the same P^{tot}, Ni/H and Si/H ratios and water abundance that produce good matches to the unzoned metal grain compositions pass through the fields of BO and CC chondrules, especially if high-temperature condensates are fractionated in the case of the CCs. While equilibrium evaporation of an alloy containing solar proportions of siderophiles into a dense impact plume is an equally plausible hypothesis for explaining the compositions of the unzoned metal grains, equilibrium evaporation can

explain CB chondrule compositions only if an implausibly large number of starting compositions is postulated. Kinetic models applied to co-condensing metal grains and silicate droplets in a region of the plume with very similar composition, but with high cooling rate and sharply declining P^{tot} during condensation, produce very good matches to the zoning profiles of Ir, Ni, Co and Cr concentrations and Fe and Ni isotopic compositions observed in the zoned metal grains in CB chondrites but produce very large positive δ^{56}Fe in the cogenetic silicate, which are not found in the chondrules.

1. INTRODUCTION

The CB (Weisberg *et al*., 2001) and CH (Weisberg *et al*., 1988) chondrites are volatile-depleted, chondritic breccias containing large proportions of angular metal grains and aggregates, chondrules or clasts with chondrule-like textures made of low-FeO silicates, exotic chondrite clasts and an interstitial metal-silicate mixture thought to have formed from a shock-produced melt. Mineral-chemical and isotopic characteristics suggest that they are related to CR chondrites (Weisberg *et al*., 2001). The CB_as, including Bencubbin, Weatherford and Gujba, contain ~60 volume % metal, cm-sized chondrules, (Fe,Ni) metal with 5-8% Ni, δ^{15}N up to ~1000‰ and rare Ca-, Al-rich refractory inclusions (CAIs). The CB_bs, including Hammadah al Hamra 237 (hereafter HH), Queen Alexandra Range 94411 (hereafter QUE), MacAlpine Hills 02675 and Isheyevo, contain ~70 volume % metal, mm-sized chondrules, (Fe,Ni) metal with 4-15% Ni, δ^{15}N up to ~200‰ and minor amounts (<1%) of CAIs. The CH chondrites, including ALH85085, NWA470, PAT91456 and PCA91467, contain 20-40 volume % metal, <100 μm-sized chondrules, metal with 4-11% Ni, δ^{15}N up to ~1500‰ and rare (<0.1%) CAIs.

Most metal grains in CB_as are homogeneous but, in CB_bs, many metal grains with more than 7-8 wt% Ni are chemically zoned, with contents of Ni and Co (Petaev *et al*., 2001) and refractory PGEs (Campbell *et al*., 2001) decreasing, Cr increasing and Pd invariant from cores to rims. These and more complex zoning profiles are found in metal grains in CH chondrites (Petaev *et al*., 2007), but many of these show chemical (Campbell and Humayun, 2004) and structural (Goldstein *et al*., 2007) characteristics of multi-stage processing, and are not considered further in this work. Chondrules in CB_as (Weisberg *et al*., 2001) and CB_bs (Krot *et al*., 2001b) have barred olivine (BO) or cryptocrystalline (CC) textures. Both types in CB_bs are strongly alkali-depleted and Mg-rich, with only 0.7-3.8 wt% FeO in CC and 1.6-5.4 wt% FeO in BO chondrules (Krot *et al*., 2001b). BO chondrules have higher CaO + Al_2O_3 contents than CCs, 10.5-22.8 wt% *vs.* <0.1-7.9 wt%.

From the covariation of Co and Ni among metal clasts in the Bencubbin CB_a, Newsom and Drake (1979) argued that the metal phase condensed from a solar gas at a total pressure, P^{tot}, ~10^{-4} bar. Meibom *et al*. (1999) and Petaev *et al*. (2001) showed that the major element zoning of metal grains in CH and CB_b chondrites, respectively, could have formed by equilibrium fractional condensation from a solar composition or modestly dust-enriched nebular region at $P^{tot}=10^{-4}$ bar. In later work, Petaev *et al*. (2003) showed that diffusive modification of such zoning profiles would have occurred if the grains condensed at a cooling rate of 10K/day, the approximate cooling rates estimated by Meibom *et al*. (1999) and Petaev *et al*. (2001). Campbell *et al*. (2001) demonstrated, however, that fractional condensation was insufficient to explain gradual, core-to-rim declines in the Ir contents of the grains, and adopted instead a model involving supersaturation and kinetically controlled growth for the zoned grains in a gas of solar

composition at P^{tot}~10^{-4} bar. Campbell *et al*. (2005) pointed out that the very slow diffusion rate of Ir in Fe-Ni alloys makes it unlikely that diffusion played a significant role in producing the Ir profiles observed by them. Furthermore, the observation by Alexander and Hewins (2004), Zipfel and Weyer (2007) and Richter *et al*. (2014) that the chemical zonation is accompanied by iron and nickel isotopic zonation from isotopically light compositions in the metal grain cores to heavier ones at their rims, is strong evidence that this metal formed by rapid disequilibrium condensation.

Campbell *et al*. (2002) found that the bulk Ir/Fe, Pd/Fe and Ni/Fe ratios in the unzoned metal grains in the CB_a chondrites are consistent with condensation from a gas whose partial pressures of siderophiles were 10^7x higher than in a gas of solar composition at P^{tot}=10^{-4} bar, and suggested that both the metal and the low-FeO, BO and CC chondrules in the CB_as condensed from a plume generated by a protoplanetary impact between a metallic and a low-FeO silicate body. Based on metal-troilite quench textures and volatile element depletions in the unzoned metal grains of the Gujba CB_a, Rubin *et al*. (2003) proposed that they formed in the same plume as both the zoned metal grains and silicate globules found in the CB_bs, but in a portion of the cloud having relatively high density compared to that for the CB_bs, despite the contrastingly modest P^{tot} and dust enrichment range previously suggested for the CB_a grains (Newsom and Drake, 1979). Krot *et al*. (2005) used ^{207}Pb-^{206}Pb dating to show that chondrules from both CB_a and CB_b chondrites formed ~5 my after CAI condensation, and concluded that the components of both types formed in a giant impact. Because this time-scale is comparable to that for accretion and differentiation of solar system planetesimals (Dauphas and Chaussidon, 2011), this opens up the possibility that one or more of the

impacting bodies was differentiated. Preferential sampling of the core of a differentiated planetesimal is a potential explanation for why CB chondrites are so metal-rich. Pierazzo *et al*. (1997) showed that the shock pressures required for vaporization of metallic iron are much greater than for dunite. Thus, in any impact involving metallic iron and silicates, it is likely that complete vaporization of silicates will accompany total vaporization of iron. Fedkin and Grossman (2013) proposed that porphyritic chondrules in ordinary chondrites formed by reaching vapor-condensed phase equilibrium in impact-generated plumes.

Since a condensation origin is required to produce the elemental and isotopic zoning of the zoned metal grains, and the Pd-Ir correlation of the unzoned metal grains can be reproduced by condensation from a post-impact vapor cloud, this manuscript seeks to determine if there is a combination of physico-chemical conditions and chemical compositions of impacting bodies, including differentiated ones, that leads to simultaneous condensation of the metal grains and chondrule-like clasts in CB chondrites from the vapor produced in the impact.

2. TECHNIQUE

2.1. Equilibrium condensation models

Condensation of the unzoned metal grains was explored using equilibrium models because their chemical compositions imply that they formed in a system containing very high partial pressures of condensable elements (Campbell *et al*., 2002), conditions conducive to establishment of gas-condensed phase equilibrium (*e.g*., Fedkin and Grossman, 2013). The VAPORS program of Ebel and Grossman (2000) was used for all

equilibrium condensation calculations, and the same thermodynamic data were used as in that work. Silicate liquids are non-ideal, and two activity-composition models are accessible in VAPORS: the CMAS model of Berman (1983); and the MELTS model of Ghiorso and Sack (1995). The former is useful for modeling refractory condensate liquids in reduced systems but it cannot be used when significant FeO contents become stable. The latter is useful for liquids containing FeO and alkalis but it cannot be used for modeling refractory liquids because it employs $CaSiO_3$ as the calcium component. This can lead to significant underestimation of the CaO contents of high-temperature liquids because SiO_2 is much less refractory than CaO. Ebel and Grossman (2000) used the CMAS model at high temperature but switched to the MELTS model at a temperature where the liquids predicted by each model separately became close in composition. This always occurred at a high enough temperature that the FeO content of the liquid was negligible. Because of the bulk compositions, relatively high dust enrichments and high pressures considered in the present work, however, the FeO content of the liquid predicted by the MELTS model sometimes becomes significant at a higher temperature than that where the compositions of the CMAS and MELTS liquids otherwise become similar to one another. Except when otherwise noted, results reported in this work are based exclusively on the MELTS model. Under circumstances where the CMAS model is expected to give more accurate liquid compositions, *i.e.*, at high temperatures where the FeO content of the liquid is <0.3 wt% and over which the SiO_2 contents predicted by the CMAS and MELTS models differ by more than 2 wt% absolute, those temperature intervals are indicated on the Figures.

Although VAPORS computes the Fe, Ni, Co, Cr and Si contents of the metal

phase at each temperature step, Pd and Ir are not included in the full equilibrium calculation. The computation is begun at sufficiently low temperatures that they are present in only trace amounts in the metal phase, so their presence does not significantly affect the proportions of major components calculated with VAPORS. The concentrations of Pd and Ir in the alloy were calculated using their atomic abundances in the plume, the ideal gas law, the total amount of condensed metal calculated by VAPORS at each temperature, and the same data used in Campbell *et al*. (2001) for vapor pressures of Pd and Ir and their activity coefficients in metallic Fe.

Campbell *et al*. (2002) suggested that the CB chondrites originated in a system that resulted from a collision between a metallic body and a reduced (low-FeO) silicate body, and this idea was tested in the present work. The metallic body was assumed to be the core of a previously impacted planetesimal whose outer, lower-density layers were lost due to tides, shock or shear (Asphaug *et al*., 2006). Because the oxygen isotopic similarity between CB and CR chondrites suggests a genetic relationship between them (Weisberg *et al*., 2001), and because the bulk metal in both chondrite types has approximately solar relative abundances of refractory siderophiles, the composition of the metallic body was assumed to be that of CR chondrite metal (Kong *et al*., 1999) in the present work. Several candidates, both chondritic and differentiated, were considered for the composition of the silicate-rich planetesimal. Low-FeO compositions investigated were that of the average H chondrite fall from Kallemeyn *et al*. (1989) and Jarosewich (1990), the average aubrite from Watters and Prinz (1979) and the terrestrial, “more refractory peridotite” from Michael and Bonatti (1985). The compositions of the Johnstown and Y75032 diogenites, the Kapoeta howardite and the Juvinas eucrite, all

taken from Mittlefehldt *et al*. (1998), were also investigated as candidates for higher-FeO, differentiated bodies. Also considered were impacts between two CR chondrite bodies whose composition was based on that of Renazzo (Mason and Wiik, 1962). In the latter calculations, the CR chondrite bodies were assumed to have been differentiated previously into core, mantle and crust, and to have had various amounts of water added to them.

The impact-generated plume was assumed to mix with residual nebular gas. The persistence of gaseous disks around stars older than 3 my (Haisch *et al*., 2001; Bergin *et al*., 2013) provides partial justification for this assumption. The extent to which nebular gas can be entrained in an outward-expanding plume of vaporized rock is not known, but the mixing ratio of such gas probably increases toward the edges of the plume. The lithophile element composition of residual nebular gas was assumed to be complementary to that of H chondrites in the calculations involving impactors of H chondrite, peridotite and achondrite compositions, and complementary to that of the CR body and its water content in collisions involving that object. In these cases, the relative abundance of an element in the gas is simply the difference between its solar abundance and its relative abundance in either H or CR composition, assuming that all of the Si was removed by the condensate. The siderophile element content of the residual nebular gas was assumed to be zero in all cases except for those involving H chondrite collisions, in which cases the residual gas was assumed to have siderophile abundances complementary to those of H chondrites. In all cases explored in this work, the system bulk compositions are so heavily dominated by dust enrichment that these small differences in residual gas composition have little effect on the calculations. The VAPORS program was used to

explore condensation from impact-generated plumes consisting of various combinations of silicate and metal enrichments relative to the residual nebular gas. An example of a silicate- and metal-enriched plume composition used in this work is given in column 5 of Table 1. When 6 wt% average H chondrite from column 2 is mixed with 5 wt% of its complementary nebular gas from column 3 and 89 wt% CR chondrite metal from column 4, the resulting plume has Ni/H and Si/H ratios that are $1.4x10^4$ and 300 times their solar values, respectively.

2.2. Kinetic condensation models

Formation of the zoned metal grains was explored with a model of kinetically controlled condensation because their chemical zoning indicates that they did not form at equilibrium, and their isotopic zoning suggests that they formed by rapid condensation. In an attempt to reproduce both the chemical and isotopic zoning of the metal grains and to take into account the Fe and Ni that would have entered the coexisting silicate droplets in the context of an impact plume model, the kinetic evaporation-recondensation model of Fedkin *et al.* (2012) was used in the present work. To calculate equilibrium vapor pressures, the model employs the Berman (1983) activity-composition model for CMAS liquids and the MELTS model of Ghiorso and Sack (1995) for multicomponent silicate liquids, and, for the present application, switches from the former to the latter when the FeO concentration in the silicate liquid rises above 0.3 wt%. The initial composition of the silicate droplet is assumed to be that of the silicate condensate assemblage that would have formed at equilibrium at the assumed nucleation temperature and the corresponding P^{tot}. Minor amounts of Fe, Ni and Cr in this initial composition were subtracted out before beginning the kinetic calculation. A 0.01 μm-radius nucleus is used to begin the

metal grain calculation. The model employs the Hertz-Knudsen equation to compute the flux of any element or isotope of interest across gas-condensed phase interfaces. In the metal alloy, the activity coefficients for Fe, Ni and Cr were the same as those used by Ebel and Grossman (2000), and those for Co, Pd and Ir were the ones used by Campbell *et al*. (2001). The same isotopic fractionation factors and evaporation coefficients for silicate liquid, and the same evaporation coefficients for metal were used as in Fedkin *et al.* (2012). In that work, isotopic fractionations of Fe were computed by writing the Hertz-Knudsen equation for each isotope, and the same procedure was adopted for both Fe and Ni in the present work. Evaporation coefficients for Ir, Pd, Co and Cr in the metal alloy were assumed to be equal to those of Fe. The evaporation coefficient for Cr in the silicate liquid was also assumed to be equal to that for Fe. The projectile and target materials were assumed to have been heated instantaneously to a temperature high enough that they evaporated completely and mixed with residual nebular gas. The system was then allowed to cool at a constant rate, from 50-150K/hr. Using a linear dependence of log P^{tot} on 1/T, P^{tot} was allowed to decline by 1-3 log units in the 500K interval following metal alloy nucleation. A system mass was considered that would yield a single silicate droplet of ~350 μm radius when all lithophiles recondensed. Given the system composition, the proportionate amount of metal was divided into a number of grains that would each have an ~200 μm radius when all siderophiles recondensed. In all cases considered, metal alloy recondensation was assumed to have been delayed until 100-150K below the equilibrium condensation temperature of pure Ir, the most refractory siderophile of those considered here. Nucleation of the silicate droplet was assumed to have been independent of the metal grains and was delayed by various amounts, ranging

up to 175K below the incoming temperature of the metal grains. The compositions of the separate metal grains and silicate droplets were each dictated solely by the Hertz-Knudsen equation, and were not equilibrated with one another. As in Fedkin *et al*. (2012), the Hertz-Knudsen equation was also used to exchange oxygen between the condensed silicate droplet and the ambient gas, causing the internal f_{O_2} of the former to equilibrate gradually with the f_{O_2} of the latter.

3. RESULTS

3.1. Equilibrium condensation from a plume made by impact between CR chondrite metal and an H chondrite

3.1.1. Metal composition

For this series of calculations, the Pd content of the average H chondrite was derived from the average Ir content of the H chondrites studied by Kallemeyn *et al*. (1989) and the mean Pd/Ir ratio of those analysed by Horan *et al*. (2003). Shown in Fig. 1 is the computed variation in composition of the metal alloy that would condense at equilibrium over a range of P^{tot} from 10^{-2} to 10^{-8} bar from a plume whose proportions of CR chondrite metal and H chondrite are such that the Ni/H and Si/H ratios are 1.4×10^4 and 300 times those of solar composition, respectively. Calculated trends of Pd/Fe (Fig. 1a) and Ir/Fe ratios (Fig. 1b) are plotted against Ni/Fe ratios for condensate metal grains and compared to solar ratios and to bulk compositions of unzoned metal grains from Bencubbin, Weatherford and Gujba (Campbell *et al*., 2002) and zoned grains from QUE. The QUE bulk compositions were calculated from Campbell *et al*.'s (2001) linear

traverses, assuming concentric zoning. The particular choice of plotted ratios is due to the fact that Campbell *et al*. (2002) found that the unzoned metal grains are enriched in both Pd and Ir relative to Fe compared to solar composition. They pointed out that redox processes could not be responsible because of the significantly greater enrichment of Ir, and showed that, in systems uniformly enriched in siderophiles, Pd can only become more refractory than Fe at very high partial pressures of siderophiles. At these Ni/H and Si/H enrichments, it is seen that lowering P^{tot} causes the composition paths in Figs. 1a and 1b to flatten significantly, such that calculated Pd/Fe and Ir/Fe ratios are much lower at the same Ni/Fe ratio at the lowest P^{tot} than at the highest one. Because of this flattening, model composition trajectories for a P^{tot} of 10^{-2}-10^{-3} bar match the bulk compositions of most unzoned metal grains and miss many of those of the zoned grains. Model composition trends calculated for a range of P^{tot} from 10^{-5} to 10^{-8} bar envelop the bulk compositions of most of the zoned metal grains in Fig. 1a and about half of those on Fig. 1b, but miss those of most of the unzoned grains. The combination of very high siderophile enrichment and high P^{tot} needed to fit the compositions of the unzoned grains confirms the finding by Campbell *et al.* (2002) that very high partial pressures of siderophiles are required.

The offsetting effects of P^{tot} and siderophile enrichment in fitting the compositions of the unzoned grains are examined in Fig. 2 for a constant Si/H enrichment of 300 relative to solar composition. At a P^{tot} of 10^{-3} bar in Figs. 2a and b, it is seen that the best fit to the unzoned grain compositions occurs for a Ni/H enrichment of $\sim 1.4 \times 10^4$ relative to solar composition, while at a P^{tot} of 10^{-2} bar in Figs. 2c and d, an equivalent fit is obtained at a Ni/H enrichment of $\sim 1.4 \times 10^3$. For a P^{tot} of 10^{-3} bar and a Ni/H

enrichment of $1.4x10^4$ relative to solar composition, even a factor of ten variation in the Si/H enrichment, from 300-3000 relative to solar composition, is seen to have a negligible effect on the fits to the unzoned metal grain compositions in Fig. 3. The lowest observed Pd/Fe and Ir/Fe ratios in the unzoned metal grains are slightly below their respective solar ratios (Anders and Grevesse, 1989) and the lowest of those in the model systems, which are at the limit of total condensation of all three elements.

3.1.2. Silicate composition

The compositions of CC and BO chondrules from CB_b chondrites (Krot *et al*., 2001a, b) are almost perfectly represented in the triangular diagram CaO + Al_2O_3-MgO-SiO_2 (Fig. 4) because the concentration of FeO, the only non-CMAS major element oxide they contain, never exceeds 5.4 wt%. As shown in Fig. 4, the CC and BO compositions lie within a range of 45-55 wt% SiO_2 along a roughly linear trend of increasing CaO + Al_2O_3 contents from CCs to BOs. Also plotted in Fig. 4, after subtraction of minor components, including FeO, and renormalization to CaO + Al_2O_3-MgO-SiO_2, is the calculated variation in bulk chemical composition of the bulk silicate assemblage that would condense at equilibrium from a plume consisting of a mixture of CR chondrite metal and H chondrite for various combinations of P^{tot}, Ni/H enrichment and Si/H enrichment investigated above. As expected from solar nebular condensation models, the bulk silicate condensate composition always begins its path at high concentrations of refractory CaO + Al_2O_3 at high temperature, heads toward the MgO corner as temperature falls, and finally increases its content of SiO_2, the most volatile of these oxides.

All of the model curves in Fig. 4 completely miss the data points for BO chondrules, passing to the low-SiO_2 side of the composition field of the latter. At constant Ni/H and Si/H enrichments of $1.4x10^4$ and 300, respectively, relative to solar composition, the silicate composition paths move closer to the BO chondrule field as P^{tot} increases from 10^{-8} to 10^{-2} bar but are still far from it at 10^{-2} bar. At constant P^{tot} and Ni/H enrichment of 10^{-3} bar and $1.4x10^4$, respectively, increasing the Si/H enrichment from 300 to $3x10^3$ relative to solar composition causes the silicate composition path to move closer to the BO field but it is still far from it at $3x10^3$. Similarly, at constant P^{tot} and Si/H enrichment of 10^{-3} bar and 300, respectively, increasing the Ni/H enrichment from $1.4x10^3$ to $1.4x10^4$ relative to solar composition moves the path no closer to the BO field and increasing it further to $1x10^5$ moves the path further away. These paths all converge when the bulk silicate reaches a SiO_2 content between 45 and 50 wt%, and evolve with sharp SiO_2 increases before crossing the CaO-, Al_2O_3-rich end of the CC chondrule trend. Neither the BO nor most of the CC chondrule compositions can be explained by equilibrium condensation from a gas made from a vaporized mixture of CR chondrite metal, H chondrite and residual nebular gas.

3.1.3. Fractionation of refractory silicates

If, however, a fraction of the Ca-, Al-rich condensate that forms at high temperature is removed from chemical communication with the vapor during continued cooling, the resulting composition trajectory cuts across the CC array at progressively lower $CaO + Al_2O_3$ contents with increasing fraction removed. Although not shown on Fig. 4, for the case of Si/H and Ni/H enrichments of 300 and $1.4x10^3$, respectively, at $P^{tot}=10^{-2}$ bar, for example, the family of trajectories created by removing the condensate

that forms at 2060K spans almost the entire range of CC chondrule compositions but the predicted compositions are lower in FeO content than the latter. No amount of removal of early condensate that forms at any temperature allows the subsequent trajectory of condensate compositions to pass through the BO chondrule compositions on Fig. 4. Thus, fractional condensation can yield the chemical compositions of neither the CC nor the BO chondrules during cooling of the vapor produced in an impact between an H chondrite and a CR metal body.

3.2. Equilibrium condensation from plumes made by impact between CR chondrite metal and various differentiated rocks and meteorites

Shown in Fig. 5 are the composition trajectories of the bulk silicate fraction of the equilibrium condensate in mixtures consisting of CR chondrite metal (Table 1), residual nebular gas (Table 1) and various types of differentiated meteorites (Table 2). In all cases shown, proportions of these components were selected to yield Ni/H and Si/H ratios of 1.4×10^3 and 300 relative to solar composition, and a P^{tot} of 10^{-2} bar was used. The conditions employed for Fig. 5 are thus very similar to those that produced good fits to the unzoned metal grain compositions in Figs. 2c and 2d.

Once again, for the plume composition made from every differentiated silicate component in Table 2, the bulk silicate composition is rich in CaO + Al_2O_3 at high temperature, and becomes more MgO- and SiO_2-rich with falling temperature. For plumes made from silicate components that are relatively low in CaO + Al_2O_3 (e.g., average aubrite, peridotite and the Johnstown and Y75032 diogenites), the composition paths pass to the low-SiO_2 side of the CB_b chondrule array, veer toward the SiO_2 corner

and then intersect the CB_b chondrule array. For plumes made from silicate components that are relatively high in $CaO + Al_2O_3$ (e.g., Kapoeta and Juvinas), the turn toward the SiO_2 corner is more gentle, and occurs at $CaO + Al_2O_3$ contents that are higher than that of the CB_b chondrule with the highest $CaO + Al_2O_3$. As a result, the latter curves do not even intersect the CB_b chondrule field. The array of chondrule compositions in CB_b chondrites cannot be explained by equilibrium condensation from a vaporized mixture of CR chondrite metal, residual nebular gas and any of the differentiated silicates investigated here.

3.3. Equilibrium condensation models in systems containing two vaporized silicate components

It was shown above that equilibrium condensation of the vapor made by an impact between CR chondrite metal and any one of many different chondritic and differentiated silicate compositions does not reproduce the bulk chemical compositions of CB_b chondrules. In general, the array of chondrule compositions lies orthogonal to the composition trajectory of the bulk silicate condensate from the vapor made from many of the investigated materials. The higher the vaporized silicate is in its $CaO + Al_2O_3$ contents, the higher is the total $CaO + Al_2O_3$ at which the evolutionary path of its condensate composition intersects the chondrule array. This suggests the possibility that the chondrule compositions could be reproduced if two different silicate compositions were vaporized in the impact, one with high and the other with low $CaO + Al_2O_3$, as long as the plume of vaporized silicates were spatially heterogeneous in composition. Perhaps the metal-rich object was differentiated into a core, and a mantle and crust with different silicate compositions from one another. In the previous sections, the metallic object was

assumed to have the composition of metal from CR chondrites because it fulfills the requirement of having solar proportions of refractory siderophiles (Kong *et al*., 1999). If it is assumed that the overall composition of each of the impacting objects was that of CR chondrites, then the vaporized silicate component of the plume would be expected to have the same isotopic composition as CR chondrites. This is an advantage, as the non-metallic fraction of CR chondrites has similar oxygen and nitrogen isotopic compositions to the silicates in CB chondrites (Weisberg *et al*., 2001).

Accordingly, it was assumed that both of the impacting bodies were CR chondrites that had become differentiated into a core, mantle and crust during the ~5 my time interval between CAI condensation and formation of CB silicates (Krot *et al*., 2005). The bulk Fe, Ni and Co contents of Renazzo (Mason and Wiik, 1962) were adjusted relative to Si to yield the solar relative proportions of Fe, Ni and Co typical of the average CR chondrite (Kong *et al*., 1999), and the S content was adjusted downward to yield the S/Fe ratio found by Rubin *et al*. (2003) for Gujba. The bulk Pd and Ir contents of Renazzo were assumed to be in solar proportion to Ni, as is the case for average CR metal (Kong *et al*., 1999). Water was assumed to have accreted onto the CR bodies hypothesized here after they differentiated, but prior to their collision. The MELTS model (Ghiorso and Sack, 1995) was applied to the resulting bulk chemical composition of Renazzo (Table 3, column 2). First, to simulate core formation, the equilibrium metal and silicate compositions were calculated at 1900K, high enough to ensure that metal and silicate phases were liquid, and log f_{O_2} =IW-2.5, chosen to yield silicates with small but non-zero FeO contents. In addition, all of the Pd and Ir in Renazzo were assumed to go into the CR core. Because the MELTS model does not compute the activity of Cr in the

metal alloy, the partitioning of Cr between metal and silicate was calculated as in Chabot and Agee (2003). For the present purposes, the metal alloy was assumed to contain no carbon and all of the inventory of S in the CR body but, because Chabot and Agee (2003) define f_{O_2} differently from MELTS, the f_{O_2} was recalculated from Equation (1) of Chabot and Agee (2003), using the mole fractions of FeO in the silicate melt and Fe in the liquid metal taken from the MELTS calculation. This calculation resulted in 29.0 wt% core and 71.0 wt% mantle, whose compositions are shown in columns 3 and 4 of Table 3, respectively. The core contains 38 % of the total Cr of the CR chondritic body.

MELTS was then applied to the CR mantle composition obtained from this calculation at 1460K and the same f_{O_2} in order to further differentiate the silicate into crust and residual mantle. At this temperature, 80% of the composition is solid, which was assumed to be the residual mantle (Table 3, column 6), and 20% is liquid, which was assumed to form the crust (Table 3, column 5). The $CaO + Al_2O_3$ content of the residual mantle is 2.1 wt% and that of the crust is 23.8 %, making the residual mantle and crust good candidates for the ($CaO + Al_2O_3$)-poor and -rich components, respectively.

3.3.1. Condensation conditions for plumes made by impacts between differentiated CR chondrite bodies

Condensation calculations identical to those in Sections 3.1 and 3.2 were performed on vaporized mixtures of CR core, CR residual mantle, CR crust and residual nebular gas compositions, all of whose compositions are in Table 3. The residual gas composition in Table 3 differs from that in Table 1 because it is assumed to be complementary to the bulk composition of the CR body (Table 3, column 2). In some

calculations, it was also assumed that water was present on the impacting bodies, and that significant amounts of this component were also added to the impact plume. When water was assumed to be present, the residual nebular gas was modified accordingly. Values of P^{tot} and the Ni/H and Si/H enrichments selected for these calculations are based on the results of Sections 3.1 and 3.2. In this model, the impact plume is assumed to be spatially heterogeneous in composition, so the entire range of proportions of CR residual mantle to CR crust was investigated. Shown in Table 3, column 8 is the bulk composition of a plume made from equal proportions of CR residual mantle and CR crust, having Ni/H and Si/H enrichments of $3x10^4$ and 500, respectively, relative to solar composition, and containing no water. Shown in the final column is the composition of a plume with the same characteristics, except that the total vaporized silicate was assumed to have contained 20 wt% water. The relative weight proportions of the vaporized components required to make these compositions are given in the footnotes to Table 3.

3.3.2. Metal condensate compositions from a plume made by impact between two differentiated CR bodies

Model metal compositions computed over a wide range of P^{tot} for the plume composition in column 8 of Table 3 are compared to bulk compositions of zoned and unzoned metal grains in CB chondrites in Figs. 6a and 6b. A curve is also shown for a case identical to the one at 10^{-2} bar except that the Ni/H enrichment was changed to $3x10^3$ relative to solar composition. Despite the different compositions of the plume components from those in Fig. 1, the fits of the Pd/Fe and Ir/Fe *vs* Ni/Fe curves for each P^{tot} to the observed metal grain compositions are nearly identical in both Figures. Although not shown, the curves for a case identical to the one at 10^{-3} bar, except that 20

wt% water was added to the total vaporized silicate (Table 3, column 9), lie on top of those for the anhydrous case. Furthermore, although also not shown, the positions of the curves for each value of P^{tot} in Fig. 6 are nearly unchanged when the ratio of CR residual mantle to CR crust varies from one extreme to the other. Once again, the compositions of most of the unzoned grains are fit well by the curves at $P^{tot}=10^{-2}$ and 10^{-3} bar, where their equilibration temperatures imply that they condensed as liquids, while those of most of the zoned grains, particularly their Pd/Fe ratios in Fig. 6a, are fit well at 10^{-5} to 10^{-8} bar, where they condense in the solid state.

Predicted Cr *vs* Ni trends for the condensate metal phase are plotted in Fig. 7a for some of the same conditions as in Fig. 6; namely, for a plume containing equal weight proportions of vaporized CR residual mantle and CR crust, a Si/H enrichment of 500 relative to solar composition and Ni/H enrichments of $3x10^4$ and $3x10^3$ at $P^{tot}=10^{-3}$ and 10^{-2} bar, respectively. The 10^{-3} bar case of Fig. 7a was explored over a wide range of CR mantle/CR crust ratios, and the results are plotted in Fig. 7b. The same cases as in Figs. 7a and 7b were run with the addition of 20 wt% water to the total silicate. In all cases, the calculated Ni content of condensate metal falls with falling temperature, while the Cr content increases, first very gradually and then more steeply, and then decreases due to the onset of co-condensation of Cr-rich spinel. In Fig. 7a, it is seen that the Cr *vs* Ni trend for the 10^{-3} bar case is displaced to lower Cr contents than that at 10^{-2} bar. The Cr *vs* Ni trends are insensitive to the relative proportions of CR crust and CR mantle (Fig. 7b). Curves for the cases with water added, though not shown, are nearly identical to the anhydrous cases. Although the Cr content of the coexisting silicate increases by a factor of 20 in the presence of water, the apparent insensitivity of the Cr concentration in the

metal to the water abundance is due to the very low absolute Cr concentration in the silicate. Most Cr is still gaseous for Ni concentrations >6.2 wt% in Fig. 7, as the temperature is above 1600K for this composition range.

For comparison in Fig. 7, bulk Cr and Ni contents are plotted only for subsets of the same, unzoned and zoned metal grains as in the previous figures. For the unzoned metal grains, this is because Campbell *et al*. (2002) measured Cr only in those from Bencubbin. For the zoned grains, only those for which electron microprobe data were obtained were used for radial averaging, as those data were of significantly higher precision than the LA-ICP-MS data (Campbell *et al*., 2001). For the unzoned grains, a wide range of Cr contents exists for a given Ni content, so it is impossible for a single curve to fit all the compositions. In Figs. 7a and 7b, it is seen that curves calculated for conditions that produce good fits to the Pd and Ir data for unzoned grains in Figs. 6a and 6b yield only fair fits to the Cr *vs.* Ni data for both the unzoned and zoned grains.

3.3.3. Condensation of silicates from a plume made by impact between two differentiated CR bodies

At conditions that produce good agreement between computed metal grain compositions and those observed for unzoned metal grains in Fig. 6, the silicate condensation sequence is relatively insensitive to P^{tot} and Ni/H enrichment but does vary in a significant way with the Si/H enrichment. This is because, in hydrogen-containing systems enriched in silicate dust, evaporation of condensed MgO and SiO_2 releases free oxygen, increasing the oxygen fugacity, f_{O_2}, in proportion to the dust enrichment. This is clearly seen in Fig. 8. In it, the log f_{O_2} relative to the iron-wüstite (IW) buffer is plotted

against temperature for enrichments of the Si/H ratio relative to solar composition of 300, 500 and $1.5x10^3$ at a P^{tot} of 10^{-3} bar and a Ni/H enrichment of $3x10^4$ for a plume containing residual nebular gas, CR core and vaporized silicate that consists of equal proportions of CR mantle and CR crust. Log f_{O_2} is always highest at high temperature, reaching IW-2.95, IW-2.5 and IW-1.5 at Si/H enrichments of 300, 500 and 1500, respectively. In each case, however, log f_{O_2} decreases sharply with falling temperature as free oxygen is consumed by recombination with gaseous Mg and SiO during recondensation of magnesium silicates. Also shown on Fig. 8 are the f_{O_2} variations for cases identical to those shown for Si/H enrichments of 300 and 500, except that 15 and 20 wt% water, respectively, was added to the silicates. Note that, compared to their respective anhydrous cases, water addition not only increases the maximum f_{O_2} at 2100K by ~0.5 log unit, but also significantly diminishes the rate of decline of f_{O_2} with decreasing temperature. At 1500K, for example, addition of these amounts of water increases the f_{O_2} by 1.1 and 1.7 log units for the 300 and 500 Si/H enrichment cases, respectively. Thus, impact plumes to which significant amounts of water have been added remain more oxidizing during cooling than anhydrous plumes because a smaller fraction of the oxidizing agent becomes sequestered in condensates.

3.3.4. Composition of silicate condensates from a plume made by impact between two differentiated CR bodies

A. Models for BO Chondrule Compositions. Shown in Fig. 9a is the variation in bulk chemical composition of the bulk silicate assemblage that would condense at equilibrium from plume regions consisting of mixtures of CR core, CR residual mantle,

CR crust and residual nebular gas in which the relative contributions of CR mantle and CR crust to the total silicate are varied. Conditions selected are those that give good fits to the unzoned grain compositions shown in Fig. 6; namely, P^{tot} of 10^{-3} bar and constant enrichments of Ni/H and Si/H of $3x10^4$ and 500, respectively, relative to solar composition. For some mixtures, curves are also shown for identical cases except that 20 wt% water was added to the total vaporized silicate, yielding a mass ratio of water/silicate of 0.25. As the relative contributions of CR crust and residual CR mantle to the total Si/H enrichment vary, it is seen that a family of condensation paths is generated. As usual, all begin at high concentrations of $CaO + Al_2O_3$ at high temperature, head toward the MgO corner as temperature falls, and finally increase their SiO_2 content sharply. As the CR mantle/total silicate ratio increases in the plume, however, the condensation paths begin their sharp increases in SiO_2 at progressively higher $MgO/(CaO + Al_2O_3)$ ratios, causing them to intersect the band of chondrule compositions at progressively lower $CaO + Al_2O_3$ contents. As a result, BO chondrule compositions lie along condensation paths for which the CR mantle contribution to the total silicate is ~40-70%, while many CC chondrule compositions lie along paths where the CR mantle contribution is 75-100%. Equilibrium condensation in plume regions in which the CR mantle fraction of the total vaporized silicate <40% cannot produce droplets with the compositions of chondrules in CB chondrites. It is also seen that, in the vicinity of the diagram where the curves cut across the array of chondrule compositions, the presence or absence of added water has little effect on the trajectories.

The calculated variation of the FeO content of the bulk silicate with its SiO_2 content is shown in Fig. 9b for some of the same plume compositions and the same P^{tot} as

in Fig. 9a, as well as for a case in which the CR mantle fraction of the total silicate is only 0.5, the Si/H enrichment is 1500 relative to solar composition, and there is no added water. Shown for comparison are the bulk compositions of the same BO and CC chondrules as in Fig. 9a. The plotted error bars are the maximum analytical errors cited by Krot *et al*. (2001b) for their defocussed electron beam analyses; those for BO chondrules are much larger than for CC chondrules.

Note that, when the Si/H enrichment is 500, the CR mantle fraction of the total silicate is 0.5 and there is no added water, *i.e.* one of the cases that passes very close to the main cluster of BO chondrule compositions in Fig. 9a, the bulk FeO content of the chondrule rises slightly, reaches a broad maximum of ~0.7 wt% and then gradually declines with progressively greater SiO_2 content. As a result, the curve misses not only the FeO contents of the BO chondrules to the low side in Fig. 9b but also the even lower FeO contents of the CC chondrules. When a higher Si/H enrichment, 1500 relative to solar composition, is used to increase the f_{O_2} without adding water to the mix, the FeO content of the bulk silicate increases sharply, reaches a maximum of 5 wt% and then declines with increasing SiO_2 content, passing through the composition field of the BO chondrules and ultimately entering the CC chondrule field as it does so. Agreement between the model predictions for these conditions and the chondrule compositions is an illusion, however. The decrease in FeO content from its peak level is not solely due to dilution by condensing SiO_2. In fact, 85% of the FeO that was present in the droplet at 40 wt% SiO_2 undergoes reduction to metallic iron with falling temperature due to the aforementioned tendency of dust-enriched systems to become much more reducing with falling temperature. This process would have led to formation of several wt% metallic

iron beads within these partially molten droplets. Such beads have never been observed inside the chondrules of CB_b chondrites.

As discussed in relation to Fig. 8 in Section 3.3.3, however, this process is overcome by addition of water to the plume in an amount that is large in comparison to the amount of oxygen released by evaporation of the silicates. In Fig. 9b, for example, results are shown for three cases spanning the range of CR mantle/total silicate ratios that pass through the cluster of BO chondrule compositions in Fig. 9a for a Si/H enrichment of 500 relative to solar composition and for which 20 wt% water was added to the total vaporized silicate. The FeO content of the bulk silicate rises to ~3.7 wt% with increasing SiO_2 concentration and passes through the field of BO chondrule compositions without any reduction of FeO with falling temperature.

Fractionation of an early, high-temperature condensate was investigated under these conditions for a plume in which the CR mantle fraction of the total silicate is 0.4. In this case, removal from further chemical communication with the vapor of 0-100% of the Ca-, Al-rich condensate that forms at 2040K yields a family of condensation trajectories that passes through the entire range of chondrule compositions on Fig. 10a and also matches the compositions of the BO chondrules on the FeO-SiO_2 plot, Fig. 10b. It is important to note that the agreement between predicted and observed FeO contents on Fig. 10b occurs in the absence of FeO reduction and in the same temperature range, 1800-1850K, as the match between predicted and observed compositions on Fig. 10a. Note that removal of high-temperature condensates from any plume region for which the CR mantle fraction of the total silicate ≤ 0.4 will produce good matches to BO chondrule compositions but, for any mantle fraction >0.4, this mechanism can account only for

those chondrules whose CaO +Al_2O_3 contents lie below the curve for that mantle fraction on Fig. 9a.

B. Models for CC Chondrule Compositions. In Fig. 11a, curves analogous to those in Fig. 9a are shown for a plume with the same components in the same proportions and P^{tot} as in that Figure, except that the Si/H enrichment is only 300 relative to solar composition. As in Fig. 9a, it is seen that curves for cases of water addition, but in an amount equal to only 15 wt% of the total vaporized silicates, yielding a water/silicate ratio of 0.176, are indistinguishable from analogous cases for which no water was added, and that the condensation trajectories for regions of the plume in which the CR mantle fraction of the total silicate ≥0.75 come closest to matching CC chondrule compositions. In Fig. 11b, curves for this combination of Si/H enrichment and water content also come very close to the field of CC chondrules, and no reduction of FeO occurs along the way. The only discrepancy between the model curves for these conditions and the CC chondrule compositions is that the model curves are slightly low in SiO_2, reaching ~52 wt%, while the chondrules range from 52 to 55 wt% SiO_2.

In Fig. 11a, for a CR mantle/total silicate ratio of 0.4, note that the BO chondrule with the highest CaO + Al_2O_3 lies very close to the condensation trajectory at 1750K. In Figs. 12a and 12b, it is seen that 95-99% removal of that particular condensate composition from further chemical communication with the gas generates composition trajectories of lower-temperature condensates that extend to higher SiO_2 contents than the curves in Figs. 11a and 11b, thus passing directly through the compositions of almost all CC chondrules in the temperature range 1710-1720K, again in the absence of reduction. This is reminiscent of the scenario envisioned by Krot *et al*. (2001a), who proposed that

CC chondrules formed by condensation of the vapor remaining after condensation of BO chondrules, except that the high-temperature condensate that was removed contains only 1 wt% FeO, lower than the lowest-FeO BO chondrule.

Satisfactory matches to the range of chondrule compositions found in CB chondrites can be attained by condensation of partially molten silicates from plume regions made by impact vaporization of differentiated CR bodies. For the entire range of BO chondrule compositions, the best matches found here are for Si/H enrichments of 500 relative to solar composition and a mass ratio of vaporized water to vaporized silicate of 0.25 (Fig. 9), either from regions whose CR mantle/total vaporized silicate ratios range from 0.4-0.7 or after sequestration of variable amounts of high-temperature, Ca-, Al-rich condensates from an initially homogeneous region in which the CR mantle contribution to the total vaporized silicate ≤40 wt%. For the entire range of CC chondrule compositions, the best matches found are for Si/H enrichments of 300 relative to solar composition and a mass ratio of water to vaporized silicate of 0.176, following sequestration of high-temperature condensates from an initially homogeneous region in which the CR mantle contribution to the total vaporized silicate ≤40 wt% (Fig. 12).

3.4. Kinetically controlled condensation of metal grains

3.4.1. Elemental zoning

The kinetic evaporation-recondensation model of Fedkin *et al*. (2012) was applied to a plume composition consisting of equal parts CR mantle and CR crust at various combinations of P^{tot}, cooling rate, degrees of subcooling of silicate and metal condensates, and enrichments in Ni/H and Si/H ratios relative to solar values. Metal alloy condensate

compositions are relatively insensitive to the specific mixture of silicate components in the impact plume, as the relative siderophile element abundances in the plume are dominated by those of the CR core component. Because Ir is so much more refractory than Fe, equilibrium condensate alloys will have much larger Ir enrichments in their cores than are observed in the zoned metal grains. As recognized by Campbell *et al*. (2001), the way to alleviate this problem is by supersaturation of the gas. Because these are such iron-rich systems, the model silicate droplet always becomes an order of magnitude more FeO-rich at relatively low H abundances, or metallic Fe-rich at relatively high H abundances, than chondrules in CB chondrites, whenever the silicate droplet is present at the temperature of appearance of the metal grains. Delaying silicate condensation to a temperature well below the onset of metal condensation circumvents this problem.

Profiles of Ir, Ni, Co and Cr concentrations calculated for condensate metal grains are compared to profiles of the same elements measured by Campbell *et al*. (2001) in zoned metal grains #1, 2 and 4 from QUE in Figs. 13a, b, c and d, respectively. The geometric mid-point of each measured profile is offset from the point of highest Ir concentration, so distance along the profiles was measured from the Ir peak. Because the three grains differ from one another in size by ~35%, data are plotted against fraction of the grain radius. The profiles were measured with an LA-ICP-MS spot diameter of ~30 μm. To facilitate comparison with the analytical data, average concentrations along successive 30 μm segments of the continuous theoretical profiles were calculated and plotted as discrete points centered 30 μm apart.

The models illustrated in Fig. 13 are for Ni/H and Si/H enrichments of 2.5×10^3 and 500, respectively, relative to solar composition, and 15 wt% water added to the total

vaporized silicate. P^{tot} is $1.6x10^{-4}$ bar at the metal nucleation temperature, but log P^{tot} varies linearly with 1/T such that P^{tot} is either 10 times (hereafter referred to as the P/10 case) or 1000 times (the P/1000 case) lower after 500K of cooling. Model parameters included a cooling rate of 50K/hr, a metal nucleation temperature of 1740K and delay of silicate condensation until 1665K. The assumed metal alloy nucleation temperature is 101K and 146K below the equilibrium condensation temperature of pure Ir (hereafter referred to as ΔT) for the P/10 and P/1000 cases, respectively. It is not known whether the selected rate of decline of temperature or pressure, the degree of metal supersaturation or the delay of the silicate liquid nucleation temperature are appropriate for the dynamical environment of a shock-generated vapor plume expanding rapidly into a relatively low-pressure ambient gas. The bulk composition of the system is seen to be close to plume compositions that produce very good agreement with compositions of unzoned metal grains in Fig. 6 but most of the condensation occurs at considerably lower P^{tot} than was employed to model the unzoned grains. In the present cases, both ending at 1238K, it is seen that both curves fit well the observed Ir and Ni profiles in Fig. 13, including the sizes of the central peaks. Both cases systematically underestimate the Co concentrations, but only by relatively small amounts. The P/10 case is low in Co by 12-15%, and the P/1000 case by only <10%. The models capture well the flatness that characterizes the observed Cr profiles from the centers of the grains outwards to 75% of their radii, and the upturn in Cr concentrations in the outer 25%. The P/10 case overestimates the steepening of the upturns at the edges by a large amount but the P/1000 case fits them well. The Cr concentrations at the edges are ~2.7 and ~1.9 times the central values in the P/10 and P/1000 cases, respectively, compared to 1.6-2.1 times in the measured grains. Increasing

P^{tot} or Ni/H enrichment by a factor of 3 or more would cause metal to nucleate above its solidus, leading to homogeneous grains. Decreasing P^{tot} or Ni/H enrichment would result in smaller central peaks and shallower profiles for Ir, Ni and Co, as would higher cooling rates and larger ΔT. Smaller ΔT would yield higher central peaks and steeper profiles.

The reason for the steepening of the computed Cr profile at the edge of the grain is that Cr is more volatile than Fe, causing the Cr concentration to build up relative to Fe at relatively low temperature. This steepening is much less extreme for the P/1000 case than for the P/10 one, making the P/1000 case is a much better fit to the measured profiles, because of the much greater rate of decline of P^{tot} for the P/1000 case. This results in a lower condensation rate at each temperature by an amount that increases with falling temperature, and in less complete condensation by the time a given temperature is reached than in the P/10 case. Because of their relative volatilities, the reduction in the degree of condensation is greater for Cr than for Fe. At 1238K, for example, 99.9% of the Fe and 99.3% of the Cr are condensed in the P/10 case but only 73% of the Fe and 49% of the Cr are condensed in the P/1000 case.

The evolution with temperature of the bulk chemical compositions of the zoned grains was computed by integration of the compositions of their successive shells for both the P/10 and P/1000 models. The resulting trajectories of Pd/Fe and Ir/Fe vs Ni/Fe ratios are plotted on Figs. 6a and 6b, respectively. It is seen that the composition paths traverse the field of the bulk compositions of the zoned grains. At 1238K, the final temperature of both model calculations, the bulk composition of the zoned metal grain in the P/10 model reaches the point of convergence of all the plotted equilibrium curves, which is the limit of total condensation of all the plotted elements. For the P/1000 model,

however, P^{tot} is so low at the end of the calculation that condensation has effectively ceased before complete condensation, so the low-temperature end of the curve is the final bulk composition of the grain. The bulk compositions computed for the measured grains suggest that many stopped growing before total condensation of these elements.

3.4.2. Fe and Ni isotopic zoning

The kinetically produced iron and nickel isotopic zonation trends computed for the model condensate metal alloy grains in Fig. 13 are shown in Figs. 14a and b, plots of $^{56}Fe/^{54}Fe$ and $^{60}Ni/^{58}Ni$ ratios, expressed as $\delta^{56}Fe$ and $\delta^{60}Ni$, respectively, *vs* distance from the center of the grain. In this Figure, the computed, continuous isotopic profiles were discretized into 30 μm-sized bins by the same procedure as used above for the concentration profiles. In both cases, $\delta^{56}Fe$ and $\delta^{60}Ni$ are -18.0 and -16.8‰, respectively, at the center and become progressively more positive toward the edge. Sequestration of light isotopes in the interior of the grain causes $\delta^{56}Fe$ and $\delta^{60}Ni$ of the coexisting vapor and, consequently, of the later-formed metal, to become progressively isotopically heavier as the temperature falls. In the P/10 case, the grain reaches 192 μm in radius, $\delta^{56}Fe$ and $\delta^{60}Ni$ in the outermost 27 μm of the grain are +20.2 and +38.4‰, respectively, and the bulk $\delta^{56}Fe$ and $\delta^{60}Ni$ of the whole grain are –1.4 and -0.86‰, respectively. Because less Fe condenses in the P/1000 case, the grain radius reaches only 172 μm, $\delta^{56}Fe$ and $\delta^{60}Ni$ in the outermost 37 μm are -4.0 and +7.0‰, and the bulk $\delta^{56}Fe$ and $\delta^{60}Ni$ of the grain are -9.4 and -5.4‰, respectively. In both cases, the greater increase in $\delta^{60}Ni$ compared to $\delta^{56}Fe$ with increasing radius is due to the fact that Ni is more refractory than Fe, so Ni is more completely condensed than Fe at any particular

temperature. Although Fe and Ni isotopic measurements are unavailable for any of the grains in Fig. 13, calculated profiles have core-rim variations similar to the ~16 and ~15‰ variations in δ^{56}Fe and δ^{60}Ni, respectively, reported by Alexander and Hewins (2004) from an HH grain, but somewhat greater than the ~10 and ~8‰ core-rim variations in δ^{56}Fe and δ^{60}Ni, respectively, seen by Richter *et al*. (2014) for grains in HH and MAC, and the 5.3‰ range in δ^{56}Fe found by Zipfel and Weyer (2007) in an HH grain. Richter *et al*. (2014) found almost no isotopic zoning in the QUE grains studied by them, despite normal elemental zoning, and attributed this to condensation from a system of unusually low mean molecular weight compared to that responsible for zoned metal grains from the other CB_bs that they studied. Nevertheless, the isotopic zoning computed here for the same conditions that produced the elemental zoning in the QUE grains in Fig. 13 is generally applicable to CB_b metal grains with the same elemental zoning.

4. DISCUSSION

4.1. Condensation of CB metal from an impact plume

Simultaneous enrichment in refractory Ir and relatively volatile Pd, both relative to Fe, compared to solar composition is a unique feature of metal grains in CB chondrites (Campbell *et al*., 2002). It was shown above (Figs. 6, 7) that the magnitudes of these enrichments, as well as the Ni and Cr contents in the unzoned grains, can be explained by equilibrium condensation from a vapor with P^{tot} of 10^{-2} bar and a Ni/H enrichment relative to solar composition of $3x10^3$, or 10^{-3} bar and $3x10^4$, respectively, regardless of the enrichment in the Si/H ratio or of the composition of the vaporized silicate. This combination of high P^{tot} and solid enrichment lies clearly outside canonical solar nebular

conditions (Fedkin and Grossman, 2013), and led Campbell *et al*. (2002) to propose that the unzoned metal grains and chondrules in CB_as condensed from a plume of matter vaporized in a protoplanetary impact. Inspection of Fig. 6 shows that, under these conditions, the compositions of the most fractionated metal grains imply that they last equilibrated with the gas at T≥1900K, indicating that the vapor from which they formed had to reach temperatures at least this high and that the grains condensed in the molten state, enhancing the likelihood that they would be homogeneous in composition. Under identical physico-chemical conditions, the same metal grain compositions can result from either equilibrium condensation or equilibrium evaporation. While there is evidence that non-equilibrium evaporation played an important role in the evolution of CAIs (Grossman *et al*., 2000), for example, evaporation into a hot, dense, impact-generated vapor plume like that envisioned here could have occurred under near-equilibrium conditions, and just such an origin has been proposed for chondrules in ordinary chondrites by Fedkin and Grossman (2013). There is little doubt that impact-generated gases can reach high temperatures, high total pressures and high dust enrichments, but it remains for detailed dynamical modeling to demonstrate whether the near-equilibrium conditions required here could have occurred in any region within a plume of matter expanding rapidly into residual nebular gas as a result of an impact between planetesimals of plausible sizes, relative velocities and porosities.

In contrast, it was seen above that elemental and isotopic zoning profiles of the zoned metal grains are best explained by rapid, non-equilibrium condensation from a region of the plume whose P^{tot} and Ni/H enrichment were lower than that of the region where the unzoned metal grains formed, and whose P^{tot} fell by as much as a factor of 10^3

over the 500K interval below the nucleation temperature of the zoned grains. The relatively steep drop in P^{tot} over this temperature range may be due to the drop in the density of the gas due to ~12% of its constituent atoms condensing as metal and silicate over this interval, and to the consequent release of their latent heat.

Fe and Ni isotopic zoning of the zoned metal grains, with progressively smaller light isotope enrichments from cores to rims, strongly suggests that they formed by rapid condensation. It was shown above that the Ir, Ni, Co and Cr concentration profiles and δ^{56}Fe and δ^{60}Ni variations across the zoned metal grains are explained well by a kinetic condensation model involving a vapor with a Ni/H enrichment of $2.5x10^3$ relative to solar composition combined with a P^{tot} varying from $1.6x10^{-4}$ bar to a factor of 10 to 10^3 less during metal alloy condensation. These conditions yield partial pressures of siderophile elements ranging from 400 to $4x10^5$ times lower than those found suitable for condensation of the unzoned metal grains, and result in condensation of siderophiles in the solid state, a phenomenon conducive to zoning at high cooling rates. The evolution of temperature with time, as well as with total pressure, is undoubtedly not the same in every part of an impact plume. Thus, it is reasonable to consider that the zoned metal grains could have formed in a separate, perhaps cooler and less dense, part of the plume from the unzoned grains, as suggested by Rubin *et al*. (2003).

4.2. Condensation of CB silicates from an impact plume

Subspherical silicate inclusions are found inside some CB_b metal grains (Weisberg *et al*., 2001). Petaev *et al*. (2007) analysed a 30 μm-diameter silicate inclusion inside Grain 8, a zoned metal grain from HH. It contains an average of 0.38 wt% Cr_2O_3

and 2.20 wt% FeO, and is enclosed between the 7.9 and 7.0 wt% Ni contours of the host metal grain. This object probably coexisted with the metal grain and was trapped within it as the metal condensed. In both the P/10 and P/1000 models discussed above, silicate condensation is delayed until the gas temperature is 75K below the nucleation temperature of metal. Over the temperature range where the metal reached the range of Ni contents observed in Grain 8, 1672-1634K in the P/10 case and 1577-1408K in the P/1000 case, the silicate droplet was 64-62% and 53-46% molten, respectively. The Cr_2O_3 and FeO contents of the co-condensing silicate droplet are predicted to reach 0.20 and 2.6 wt%, respectively, in the P/10 case and 0.34 and 3.8 wt%, respectively, in the P/1000 case. These values, especially for the P/1000 case, are in quite good agreement with the measurements of Petaev *et al*. (2007), providing important confirmation of the relevance of the model parameters.

The zones of a metal grain with this range of Ni contents would be expected to have δ^{56}Fe of -7.5 to +4.5‰, with a mean of -2.1‰ in the P/10 case; the values for δ^{60}Ni would be +0.12 to+20.9‰, with a mean of +9.4‰. In the P/1000 case, δ^{56}Fe would range from -5.4 to +3.0‰, and average -1.7‰; the values for δ^{60}Ni would be +5.7 to +17.0‰, and average +11.6‰. Because the metal grain and silicate droplet do not equilibrate with one another, they do not have the same isotopic composition. While the metal grain sequesters relatively light Fe and Ni in buried shells of material, the liquid droplet is assumed to homogenize its isotopic composition. Thus, while both the metal grain and the coexisting silicate droplet are immersed in a common gas, the isotopic composition of the grain surface differs from that of the droplet, causing differences in the relative net fluxes of the isotopes. Therefore, by the time the Ni content of the metal

grain falls to 7 wt%, δ^{56}Fe of the silicate droplet is +17.4‰ and +7.6‰ in the P/10 and P/1000 cases, respectively. Iron isotopic measurements of such silicate inclusions would provide an obvious test of the model presented herein. Those objects should have highly anomalous Fe isotopic compositions, distinct from those of the surrounding metal phase.

The bulk chemical compositions of CB chondrites call for their origin in extremely iron-rich systems; yet, the chondrules in these meteorites are quite low in total iron, containing no metallic Fe and only a few wt% FeO. The difficulty of preventing buildup of large iron concentrations in silicate droplets that nucleated at temperatures close to the nucleation temperature of the zoned metal grains was alluded to in Section 3.4.1. In such iron-rich systems as these, there is an enormous flux of iron atoms to the surface of the silicate droplet, unless nucleation of the silicate occurs well below the nucleation temperature of the metal grains, by which time a large fraction of the iron has become sequestered inside the latter. The problem with this mechanism is that the process for sequestering iron inside the zoned metal grains causes it to have large negative δ^{56}Fe (*e.g.*, Fig. 14), leading to very large positive δ^{56}Fe in the residual gaseous iron and thus in the iron that subsequently condenses into the silicates, as seen above. Such silicates will almost always have much higher δ^{56}Fe than the values reported for individual Gujba chondrules, 0.01-0.90‰ (Tang and Dauphas, 2012) and silicate separates from Bencubbin, Gujba and Isheyevo, 0.07-0.27‰ (Zipfel and Weyer, 2007).

While the kinetic model presented in this work provides a reasonable explanation of the chemical and isotopic composition of the zoned metal grains, the predicted δ^{56}Fe of cogenetic silicate droplets would be quite distinct from those of the coexisting

chondrules in the CB chondrites. In conclusion, the silicate chondrules in these meteorites did not form in the same region of the plume as the zoned metal grains. Except for the relatively small amount of silicate that became trapped inside the zoned metal, almost all silicate condensates present in the region of the plume where the zoned metal grains formed became separated from the metal grains before they accreted.

On the other hand, it was demonstrated above that, under the conditions of formation of the unzoned metal grains, partially molten silicate droplets would be expected to condense with mineralogical and chemical compositions like those of CB chondrules, as suggested by Campbell *et al*. (2002) and Rubin *et al.* (2003). The conditions required are that the ratio of vaporized metal to vaporized silicate was ~6-100 times the solar ratio, that a Ca-, Al-rich and a Ca-, Al-poor silicate component were distributed heterogeneously within this part of the impact plume, and that the weight ratio of vaporized water to vaporized silicate was ~0.176-0.25. Under the same physico-chemical conditions, equilibrium evaporation would be expected to produce the same silicate compositions if the droplets last equilibrated with the vapor at ~1800K for the BO chondrules (Fig. 9) and ~1600K for the CCs (Fig. 11). Although such an origin in a dense impact plume was proposed for chondrules in ordinary chondrites by Fedkin and Grossman (2013), all chondrule compositions considered in that work could be achieved by minimal evaporation of a starting material containing chondritic proportions of condensables. In the case of CB chondrule formation by equilibrium evaporation, however, a wide range of non-chondritic starting compositions would be required, lying at more SiO_2-rich compositions than the chondrules themselves, along extensions of the condensation curves illustrated in Figs. 9 and 11.

Zipfel and Weyer (2007) and Tang and Dauphas (2012) measured $\delta^{56}Fe$ in coexisting metal and chondrule fractions separated from Bencubbin and Gujba, CB_as in which there are no zoned metal grains. For Bencubbin, Zipfel and Weyer (2007) found that $\delta^{56}Fe$ is -0.2‰ and +0.3‰ in metal and silicates, respectively, and in Gujba -0.4‰ and +0.1‰, respectively. In Gujba, Tang and Dauphas (2012) found that $\delta^{56}Fe$ ranged from -0.06 to -0.17‰, averaging -0.12‰, in three metal globules, and from +0.01‰ to +0.90‰, averaging +0.34‰, in 14 silicate chondrules. $\delta^{56}Fe$ is consistently negative in the unzoned metal grains and consistently positive in the silicates, suggesting a complementary relationship between the two phases, but the magnitudes of the mass-fractionations in the unzoned metal grains are much smaller than in the zoned ones. It is conceivable that, even at the relatively high partial pressures of iron envisioned for the region of the impact plume where the unzoned grains formed, the speed with which the metallic iron condensed could have resulted in negative $\delta^{56}Fe$ excursions which were not totally erased by subsequent condensation, especially if cooling and/or accretion were rapid. In the previously described models for condensation of unzoned metal grains, oxidized iron in the silicates is predicted to form by direct condensation from the last gaseous iron remaining after almost all of the metallic iron has condensed. If the unzoned metal grains condensed with slightly negative $\delta^{56}Fe$, perhaps the relatively small positive values of $\delta^{56}Fe$ observed in CB silicates are the natural result of condensation of this complementary, thus slightly isotopically heavy, gaseous iron. In any event, the negative $\delta^{56}Fe$ of the unzoned metal grains argues against their being evaporation residues.

4.3. Compositions of the two silicate components

4.3.1. Major elements

The advantages of assuming that the impact plume contains the vapor from two contrasting silicate compositions were demonstrated in Section 3.3. When one silicate component is rich and the other poor in $CaO + Al_2O_3$, the major element compositions of BO and CC chondrules can be explained by condensation from distinct regions of the plume that differ in their mixing proportions of the two silicate components, as seen in Figs. 9 and 11. If one silicate composition were from deep within the impacting bodies and the other from shallow regions, such variation in their relative proportions within the plume would be expected to result from the spatial variation of peak pressure in the impact zone (Melosh, 1989).

While applying a one-stage equilibrium melting model to the CR chondrite body may be a gross oversimplification of the complexity of small-body differentiation, fractionation of the chondritic silicate portion of the body into 20% liquid and 80% residual solid at 1460K does yield a relatively CaO-, Al_2O_3-poor, mafic mantle, consisting of olivine, orthopyroxene and spinel, and a relatively CaO-, Al_2O_3-rich, felsic crust, made mostly of plagioclase, clinopyroxene and silica. The computed CaO/Al_2O_3 weight ratios of crust and residual mantle are 0.72 and 0.85, below and above the solar ratio of 0.79, respectively. It was found in Section 3.3.4. that plume compositions that yield the best matches to the compositions of CB chondrules are enriched in crust relative to mantle compared to the overall CR body. For plume regions whose compositions have crustal weight fractions of the total vaporized silicates of 0.3 and 0.6, typical of those that yield good matches to the compositions of CC and BO chondrules, respectively, the CaO/Al_2O_3 weight ratios are 0.74 and 0.73, both below the solar ratio. Even when

modeling chondrule compositions by fractional removal of high-temperature condensates from such regions, removal temperatures were selected such that both Ca and Al were totally condensed in the refractory condensates, thus preserving these subchondritic ratios in the chondrules that formed from the remaining material. Krot *et al.* (2001b) measured bulk compositions of CB chondrules by defocused electron beam analysis. Although the data are widely scattered and the uncertainties large, especially for the CC chondrules, the average CaO/Al_2O_3 weight ratio of the BO chondrules is 0.70, in good agreement with the above model value, 0.73. Because the error bar on the CaO/Al_2O_3 weight ratio of almost every CC chondrule overlaps the model value of 0.74, the model is also in good agreement with their compositions.

4.3.2. Oxygen isotopes

On a graph of $\delta^{17}O$ *vs* $\delta^{18}O$, the oxygen isotopic compositions of components of CR chondrites plot on a unique mixing line, along which the δ-values increase with increasing petrographic evidence of hydrous alteration (Weisberg *et al*., 1993). Among the analysed components, the least altered appear to be olivine and pyroxene separates from Renazzo that average $\delta^{18}O$ = -0.18 and $\delta^{17}O$ = -2.4‰. Oxygen isotopic compositions of bulk CB chondrites form a linear array just below the CR mixing line (Weisberg *et al*., 2001), and the average whole-rock analysis of four of them, $\delta^{18}O$ = 1.7 and $\delta^{17}O$ = -1.4‰, is only slightly displaced from the Renazzo separates. This similarity in oxygen isotopic composition would be expected if the two colliding bodies envisioned here were of CR chondrite composition. This is because, in the plume composition shown in column 9 of Table 3, for example, 67.1 atomic % of the oxygen derives from

vaporized CR silicates, and 32.6% from CR water. Although 0.3 atomic % of the oxygen comes from the residual nebular gas, it is difficult to assess what the oxygen isotopic composition of such matter would have been five million years after CAI condensation.

In Section 3.3.4., it was found that one way of generating CB chondrule compositions is by sequestering from further reaction with the gas early, high-temperature condensates that lie along the CaO-, Al_2O_3-rich parts of the condensation trajectories in Figs. 10a and 11a. It is important to note that, along these paths, the MgO content remains low, ~1 wt %, while the SiO_2 content rises from ~10 to 30 wt %. Although CAIs are rare to minor constituents of CB chondrites, those analysed by Krot *et al*. (2001b) have much lower SiO_2/MgO ratios than the model plume condensates. As a result, none of the sequestered high-temperature condensates have major element compositions like any of the CB CAIs. Furthermore, the sequestered objects would have oxygen isotopic compositions derived from those of CR chondrites, while the oxygen isotopic compositions of the CB CAIs lie along the CCAM line (Krot *et al*., 2001b). These CAIs are therefore general solar nebular material, not cogenetic with the chondrules in these meteorites, whose oxygen isotopic compositions lie just below the CR mixing line, resolvably above the CCAM line (Weisberg *et al*., 2001). Any Ca-, Al-rich condensates that were removed from further interaction with plume gases at high temperature were apparently not accreted into the CB chondrites.

4.3.3. Rare earth elements

Given the mineralogical contrast between CR crust and mantle, it is likely that the REE would have been nearly quantitatively extracted into the liquid that formed the crust,

which would then have a flat, chondrite-normalized REE pattern. Thus, in a collision between two differentiated CR chondrite bodies, a plume made only of vaporized CR crust would be expected to have a flat REE pattern, and any addition of vaporized CR residual mantle to the plume would simply dilute the abundances. In this way, the absolute REE abundances in a region of the plume would have decreased with increasing proportions of CR mantle therein. Because the REE are expected to have condensed totally along with CaO and Al_2O_3 at high temperature before most of the MgO and SiO_2, chondrules that condensed from the plume would be expected to have flat REE patterns with enrichments that correlate with their contents of CaO + Al_2O_3. This is in agreement with REE measurements of CC and BO chondrules (Krot *et al.,* 2001b).

4.4. Relative Proportions of Vaporized Components

The requirement that significant water be present in the impact plume was discussed in Section 3.3.4. In Fig. 9b, it was shown that, if a plume is enriched in vaporized, anhydrous CR silicates to a Si/H ratio of 1500 relative to solar composition, the FeO content of the silicate droplets that condense from it at high temperature is comparable to the highest FeO, 5.4 wt%, seen in CB chondrules. It was also shown that, upon cooling, much of that FeO undergoes reduction to metallic Fe, beads of which have never been observed within CB chondrules. For a plume with the same Si/H enrichment, however, if the silicates contain sufficient water to prevent reduction of FeO, the FeO content of the droplets would be much higher than found in CB chondrules. Calculations like those used for Fig. 9b, but for many combinations of Si/H enrichments and water contents, were used to constrain the range of possible Si/H enrichments that would reproduce the FeO contents of CB chondrules. It was found by trial and error that, to

constrain the FeO content of the condensing silicate droplet to ≤5.4 wt %, the maximum Si/H enrichment is 600 relative to solar composition for any plume with sufficient water in it to prevent subsequent reduction of the FeO. The highest bulk water content reported by Weisberg *et al.* (1993) for CR chondrites is equivalent to ~10 wt% of the silicate fraction. At the maximum Si/H enrichment needed to match the highest FeO content of CB chondrules, the water content of the vaporized silicates needed to prevent reduction is 20 wt%, within a factor of two of this amount. Due to its much greater volatility than the other vaporized components, water may have been evaporated from a much greater volume of the matter heated by the impact, leading to enhancement of the water abundance in the plume from which the CB chondrites condensed. If 20 wt% is the maximum water content considered reasonable for the vaporized silicate, the minimum Si/H enrichment that allows a match to the lowest FeO contents, ~0.7 wt%, of CB chondrules in the absence of FeO reduction is 300 relative to solar composition.

Unless some residual nebular gas mixes with the vaporized silicate, results of the present calculations would be very similar to the infinite dust enrichment cases of Fedkin and Grossman (2013). Plume condensates from vaporized anhydrous silicates and vaporized silicates containing 20 wt% water would resemble those from vaporized H' and CI dust, respectively, in that work. At high temperature, such condensate droplets would contain ~15 and ~35 wt% FeO, respectively. In the case of anhydrous dust, a very large fraction of the initial FeO would undergo reduction with falling temperature. In the case of the water-containing dust, the FeO content would remain very high. In neither case would the resulting droplets resemble CB chondrules.

The tradeoff between P^{tot} and Ni/H enrichment was discussed in Section 3.1.1. in

the context of fitting the Pd/Fe and Ir/Fe *vs* Ni/Fe data for the unzoned metal grains. In Figs. 6a and 6b, equivalent fits to the data points are achieved for a P^{tot} and Ni/H enrichment of 10^{-2} bar and $3x10^3$ relative to solar composition, respectively, as for the combination of 10^{-3} bar and $3x10^4$. If P^{tot} were only 10^{-4} bar, a gigantic Ni/H enrichment of $3x10^5$ would be required and, if a more modest Ni/H enrichment of 300 prevailed, a more substantial plume P^{tot} of 10^{-1} bar would be required for equivalent fits. Choosing an intermediate range of P^{tot}, 10^{-2} to 10^{-3} bar, as the most reasonable leads to a Ni/H enrichment in the range of $3x10^3$ to $3x10^4$ relative to solar composition.

The Si/H enrichments derived above for CB chondrule formation, 300-600 relative to solar composition, could have coexisted in the same plume region with the optimum Ni/H enrichments needed to account for the compositions of the unzoned metal grains. Total condensation of a plume region with Ni/H enrichments of $3x10^3$ and $3x10^4$ would lead to end products containing 64-78 and 94-97 wt% metal, respectively. It is interesting that independent assessments of the Si/H and Ni/H enrichments, if characteristic of the same plume region, lead to condensation products with metal contents so similar to the 81 to 87 wt% estimates derived from literature reports of the volume % of metal in the CB_a and CB_b chondrites, respectively. This suggests that the unzoned metal grains and chondrules condensed from a common region of the plume.

When differentiated, the model CR bodies considered in this work consist of 29.0 wt% core and 71.0 wt% silicate. The latter, in turn, is differentiated into 80.0 wt% residual mantle and 20.0 wt% crust. The relative proportions of core and silicate are quite distinct from those found here for co-condensation of unzoned metal grains and chondrules, *i.e.*, a very large oversampling of core relative to silicate occurred. While the

best matches to CC chondrule compositions are for CR mantle fractions of the total silicate as high as 0.75, similar to the mantle fraction of the total silicate in the CR body, some BO chondrule compositions require mantle fractions at least as low as 0.40, which represents a significant enrichment of the plume in crust relative to mantle.

Because of the variation of impact temperatures and pressures with depth, and differences in material properties between metal and silicates, these components may not have been vaporized in the same proportions as existed in the pre-impact bodies. Furthermore, during an early solar system period of high collision frequencies among differentiated protoplanets, many of these objects may have been totally destroyed by physical disruption and vaporization, and then reconstituted by recondensation and reaccretion. Such objects would have undergone dramatic changes in their bulk compositions as a result. Asphaug *et al*. (2006) and Leinhardt and Stewart (2012) discussed particular mechanisms for stripping of surface layers, particularly during grazing impacts, and Yang *et al*. (2007; 2010) presented evidence from specific iron meteorite types for near-total removal of silicate mantles from planetary cores by protoplanetary collisions. Perhaps one or both of the differentiated CR bodies envisioned here underwent earlier collisions that resulted in stripping of their original silicates and reaccretion of small amounts of their original mantle and crustal material in different proportions from those originally present. Marty *et al*. (2010) showed that energetic impacts continued to affect Bencubbin up until 4.2 Ga ago, long after recondensation and reaccretion of its components.

4.5. Uniqueness of Mixing Components

In this work, conditions were found that yield the chemical and isotopic compositions of CB metal and silicates by condensation from a plume generated by impact vaporization of two differentiated bodies of CR chondrite composition. If the oxygen and nitrogen isotopic compositions of CB chondrites are ignored, however, it is apparent that the chemical compositions of CB metal and silicates can be accounted for in plumes generated by impacts involving bodies of compositions other than CR chondrites. In particular, a metal core from any body with chondritic proportions of non-volatile siderophiles could serve as a metallic impactor, as long as core separation occurred at sufficiently low f_{O_2} that it contained several tens of % of the planetary Cr inventory, for plumes with Ni/H enrichments of the magnitude envisioned here. Furthermore, any body with a Ca/Al ratio and relative proportions of REE that are nearly chondritic, and that differentiated into a mantle and a crust into which Ca, Al and REE were nearly totally extracted, could serve as a silicate impactor. In order to satisfy the additional oxygen and nitrogen isotopic constraints, however, two differentiated CR chondrite bodies were selected for this study.

5. CONCLUSIONS

If a CR chondrite body is differentiated into core, relatively CaO-, Al_2O_3-poor mantle and CaO-, Al_2O_3-rich crust, and later accretes significant amounts of water, a collision between it and an identical body can produce impact vapor with an appropriate chemical composition for condensation of CB metal grains and chondrules. Good matches to the compositions of the unzoned metal grains in CB chondrites are obtained by equilibrium condensation or evaporation in a region of the plume having P^{tot} and an

enrichment in Ni/H relative to solar composition of 10^{-2} bar and $3x10^3$, respectively, or 10^{-3} bar and $3x10^4$, respectively. From this gas, good matches to the compositions of BO chondrules are obtained when the Si/H enrichment is 500, the water abundance is 20 wt% and the mantle component is either 40-70 wt% of the total vaporized silicate or if refractory condensate fractionation occurs with a mantle fraction ≤40%. CC chondrule compositions arise from regions where the Si/H enrichment is 300, the water abundance is 15 wt% of the total vaporized silicate and refractory condensate separation occurs where the mantle fraction of the total silicate ≤40 wt%. An origin for the chondrules by equilibrium evaporation is unlikely due to the wide range of starting compositions that would be required. Kinetic models applied to co-condensing metal grains and silicate droplets in a region of the plume with very similar composition, but with high cooling rate and sharply declining P^{tot} during condensation, produce very good matches to the zoning profiles of Ir, Ni, Co and Cr concentrations and Fe and Ni isotopic compositions that are observed in the zoned metal grains in CB chondrites, but produce very large positive $\delta^{56}Fe$ and $\delta^{60}Ni$ in the cogenetic silicate. Because such isotopic fractionations are not found in CB chondrules, the latter are most likely cogenetic with the unzoned metal grains. Condensation from a plume of impact vapor is a viable hypothesis for making all the metal grains and chondrules of CB chondrites, but whether the required physico-chemical conditions and their spatial variation can be attained in such a setting must be addressed by detailed dynamical modeling.

Acknowledgments-We thank N. Artemieva, F. Ciesla, B. Johnson and H. J. Melosh for insight into impact processes, and A. S. Colman, N. Dauphas, and M. Weisberg for helpful discussions. Reviews by M. Petaev and an anonymous reviewer led

to important improvements to the paper. This work was supported by funds from the National Aeronautics and Space Administration under grants NNX08AE06G and NNX13AE73G to LG and NNX13AI06G to MH, as well as funds from the National Science Foundation under grant EAR-1427123 to AJC.**REFERENCES**

Alexander C. M. O'D. and Hewins R. H. (2004) Mass fractionation of Fe and Ni isotopes in metal in Hammadah al Hamra 237 (abstract). *Meteoritics Planet. Sci*. **39**, A13.

Anders E. and Grevesse N. (1989) Abundances of the elements: meteoritic and solar. *Geochim. Cosmochim. Acta* **53**, 197–214.

Asphaug E., Agnor C. B., and Williams Q. (2006) Hit-and-run planetary collisions. *Nature*, **439**, 155-160.

Bergin E. A., Cleeves L. I., Gorti U., Zhang K., Blake G. A., Green J. D., Andrews S. M., Evans II N. J., Henning T., Öberg K., Pontoppidan K., Qi C., Salyk C., van Dishoeck E. F. (2013) An old disk still capable of forming a planetary system. *Nature*, **493**, 644-646.

Berman R. G. (1983) A Thermodynamic Model for Multicomponent Melts, with Application to the System CaO-MgO-Al_2O_3-SiO_2. Ph.D. dissertation, Univ. of British Columbia.

Campbell A. J. and Humayun M. (2004) Formation of metal in the CH chondrites ALH 85085 and PCA 91467. *Geochim. Cosmochim. Acta* **68**, 3409-3422

Campbell A. J., Humayun M., Meibom A., Krot A. N., and Keil K. (2001) Origin of zoned metal grains in the QUE94411 chondrite. *Geochim. Cosmochim. Acta* **65**, 163–180.

Campbell A. J., Humayun M. and Weisberg M.K. (2002) Siderophile element constraints on the formation of metal in the metal-rich chondrites Bencubbin, Weatherford, and Gujba. *Geochim. Cosmochim. Acta*, **66**, 647-660.

Campbell A. J., Humayun M. and Weisberg M. K. (2005) Compositions of unzoned and zoned metal in the CB_b chondrites Hammadah al Hamra 237 and Queen Alexandra Range 94627. *Meteoritics Planet. Sci.* **40**, 1131-1148.

Chabot N. L. and Agee C. B. (2003) Core formation in the Earth and Moon: New experimental constraints from V, Cr, and Mn. *Geochim. Cosmochim. Acta*, **67**, 2077-2091.

Dauphas N. and Chaussidon M. (2011) A perspective from extinct radionuclides on a young stellar object: The sun and its accretion disk. *Ann. Rev. Earth Planet. Sci.*, **39**, 351-386.

Ebel D. S. and Grossman L. (2000) Condensation in dust-enriched systems. *Geochim. Cosmochim. Acta* **64**, 339–366.

Fedkin A. V. and Grossman L. (2013) Vapor saturation of sodium: Key to unlocking the origin of chondrules. *Geochim. Cosmochim. Acta* **112**, 226–250.

Fedkin A. V., Grossman L., Ciesla F. J. and Simon S. B. (2012) Mineralogical and isotopic constraints on chondrule formation from shock wave thermal histories. *Geochim. Cosmochim. Acta* **87**, 81–116.

Ghiorso M. S. and Sack R. O. (1995) Chemical mass transfer in magmatic processes IV. A revised and internally consistent thermodynamic model for the interpolation and

extrapolation of liquid-solid equilibria in magmatic systems at elevated temperatures and pressures. *Contrib. Mineral. Petrol.* **119**, 197-212.

Goldstein J. I., Jones R. H., Kotula P. G. and Michael J. R. (2007) Microstructure and thermal history of metal particles in CH chondrites. *Meteoritics Planet. Sci*. **42**, 913-933.

Grossman L., Ebel D. S., Simon S. B., Davis A. M., Richter F. M. and Parsad N. M. (2000) Major element chemical and isotopic compositions of refractory inclusions in C3 chondrites: The separate roles of condensation and evaporation. *Geochim. Cosmochim. Acta* **64**, 2879-2894.

Haisch Jr. K. E., Lada E. A. and Lada C. J. (2001) Disk frequencies and lifetimes in young clusters. *Astrophys. J.* **553**, L153-L156.

Horan M. F., Walker R. J., Morgan J. W., Grossman J. N. and Rubin A. E. (2003) Highly siderophile elements in chondrites. *Chem. Geol.* **196**, 5-20.

Jarosewich E. (1990) Chemical analyses of meteorites: A compilation of stony and iron meteorite analyses. *Meteoritics* **25**, 323– 337.

Kallemeyn G. W., Rubin A. E., Wang D. and Wasson J. T. (1989) Ordinary chondrites: Bulk compositions, classification, lithophile-element fractionations, and composition-petrographic type relationships. *Geochim. Cosmochim. Acta* **53**, 2747-2767.

Kong P., Ebihara M., and Palme H. (1999) Distribution of siderophile elements in CR chondrites: Evidence for evaporation and recondensation during chondrule formation. *Geochim. Cosmochim. Acta* **63**, 2637-2652.

Krot A. N., Meibom A., Russel S.S., Alexander C.M.O'D, Jeffries T.E., and Keil K. (2001a). A new astrophysical setting for chondrules formation. *Science*, **291**, 1776-1779.

Krot A. N., McKeegan K. D., Russell S. S., Meibom A., Weisberg M. K., Zipfel J., Krot T. V., Fagan T. J. and Keil K. (2001b). Refractory calcium-aluminum-rich inclusions and aluminum-diopside-rich chondrules in the metal-rich chondrites Hammadah al Hamra 237 and Queen Alexandra Range 94411. *Meteoritics Planet. Sci*. **36**, 1189-1216.

Krot A. N., Amelin Yu., Cassen P. and Meibom A. (2005) Young chondrules in CB chondrites from a giant impact in the early Solar System. *Nature*, **436**, 989-992.

Leinhardt Z. M. and Stewart S. T. (2012) Collisions between gravity-dominated bodies. I. Outcome regimes and scaling laws. *Astrophys. J.* **745**, 79-105.

Marty B., Kelley S. and Turner G. (2010) Chronology and shock history of the Bencubbin meteorite: A nitrogen, noble gas, and Ar-Ar investigation of silicates, metal and fluid inclusions. *Geochim. Cosmochim. Acta* **74**, 6636-6653.

Mason B. and Wiik H. B. (1962) The Renazzo meteorite. *Amer. Mus. Novitates* 2106.

Meibom A., Petaev M. I., Krot A. N., Wood J. A. and Keil K. (1999) Primitive FeNi metal grains in CH carbonaceous chondrites formed by condensation from a gas of solar composition. *J. Geophys. Res*. **104**, 22053-22059.

Melosh H. J. (1989) *Impact Cratering: A Geological Process*. Oxford University Press, 256 pp.

Michael P. J. and Bonatti E. (1985) Peridotite composition from the North Atlantic: regional and tectonic variations and implications for partial melting. *Earth Planet. Sci. Lett.*, **73**, 91-104.

Mittlefehldt D. W., McCoy T. J., Goodrich C. A., Kracher A. (1998) Non-chondritic meteorites from asteroidal bodies. In *Planetary Materials*. (ed. J. J. Papike), *Revs. Mineralogy* **36**, pp. 4-1–4-195. Mineralogical Society of America, Washington, D.C.

Newsom H. E. and Drake M. J. (1979) The origin of metal clasts in the Bencubbin meteoritic breccia. *Geochim. Cosmochim. Acta* **43**, 689-707.

Petaev M. I., Meibom A., Krot A.N., Wood J.A., and Keil K. (2001) The condensation origin of zoned metal grains in Queen Alexandra Range 94411: Implications for the formation of the Bencubbin-like chondrites. *Meteoritics Planet. Sci.*, **36**, 93-106.

Petaev M. I., Wood J. A., Meibom A., Krot A. N. and Keil K. (2003) The ZONMET thermodynamic and kinetic model of metal condensation. *Geochim. Cosmochim. Acta* **67**, 1737-1751.

Petaev M. I., Ivanova M. A., Krot A. N., Meibom A. and Jacobsen S. B. (2007) Different zoning patterns in metal grains from the CH and CB_b chondrites: evidence for a complicated cooling history of their nebular source regions. *Lunar Planet. Sci*. **XXXVIII**, #1641.

Pierazzo E., Vickery A. M. and Melosh H. J. (1997) A reevaluation of impact melt production. *Icarus* **127**, 408-423.

Richter F. M., Huss G. R. and Mendybaev R. A. (2014) Iron and nickel isotopic

fractionation across metal grains from three CB_b meteorites. *Lunar Planet. Sci*. **XLV**, #1346.Rubin A. E., Kallemeyn G. W., Wasson J. T., Clayton R. N., Mayeda T. K., Grady M., Verchovsky A. B., Eugster O. and Lorenzetti S. (2003) Formation of metal and silicate globules in Gujba: a new Bencubbin-like meteorite fall. *Geochim. Cosmochim. Acta* **67**, 3283–3298.

Tang H. and Dauphas N. (2012) Abundance, distribution, and origin of ^{60}Fe in the solar protoplanetary disk. *Earth Planet. Sci. Lett.* **359-360**, 248-263.

Watters T. R. and Prinz M. (1979) Aubrites: Their origin and relationship to enstatite chondrites. In *Proc. 10th Lunar Planet. Sci. Conf*., Lunar Planet. Inst., Houston, TX, pp. 1073-1093.

Weisberg M. K., Prinz M. and Nehru C. E. (1988) Petrology of ALH85085: a chondrite with unique characteristics. *Earth Planet. Sci. Lett*. **91**, 19-32.

Weisberg M. K., Prinz M. and Nehru C. E. (1990) The Bencubbin chondrite breccia and its relationship to CR chondrites and the ALH85085 chondrite. *Meteoritics* **25**, 269-279.

Weisberg M. K., Prinz M., Clayton R. N. and Mayeda T. K. (1993) The CR (Renazzo-type) carbonaceous chondrite group and its implications. *Geochim. Cosmochim. Acta* **57**, 1567-1586.

Weisberg M. K., Prinz M., Clayton R.N., Mayeda T.K., Sugiura N., Zashu S. and Ebihara M. (2001) A new metal-rich chondrite grouplet. *Meteoritics Planet. Sci.* **36**, 401-418.

Yang J., Goldstein J.I. and Scott E.R.D. (2007) Iron meteorite evidence for early formation and catastrophic disruption of protoplanets. *Nature* **446**, 888-891.

Yang J., Goldstein J.I., Michael J.R., Kotula P.G. and Scott E.R.D. (2010) Thermal history and origin of the IVB iron meteorites and their parent body. *Geochim. Cosmochim. Acta* **74**, 4493-4506.

Zipfel J. and Weyer St. (2007) In situ analysis of Fe isotopes in zoned metal grains of Hammadah al Hamra 237. *Lunar Planet. Sci*. **XXXVIII**, #1927.

FIGURE CAPTIONS

Fig. 1. Computed variation of the bulk (a) Pd/Fe and (b) Ir/Fe ratio with the bulk Ni/Fe ratio for metal grains that condense at equilibrium from a vaporized mixture of CR chondrite metal, H chondrite and residual nebular gas having enrichments in Ni/H and Si/H of 1.4×10^4 and 300, respectively, relative to solar composition at a variety of total pressures. Theoretical curves are compared to bulk compositions of unzoned metal grains in Bencubbin, Gujba and Weatherford (Campbell *et al*., 2002) and zoned metal grains in QUE, the latter calculated from traverses across the grains (Campbell *et al*., 2001). Numbers on the curves are temperatures in K. The star marks the composition of a metal alloy having solar proportions of Fe, Ni, Pd and Ir (Anders and Grevesse, 1989).

Fig. 2. Computed variation of the bulk (a, c) Pd/Fe and (b, d) Ir/Fe ratio with the bulk Ni/Fe ratio for metal grains that condense at equilibrium from a vaporized mixture of CR chondrite metal, H chondrite and residual nebular gas with a Si/H enrichment of 300 relative to solar composition and total pressures of (a, b) 10^{-3} bar and (c, d) 10^{-2} bar at a variety of Ni/H enrichments. Theoretical curves are compared to the same measured data as in Fig. 1. Numbers and symbols as in Fig. 1.

Fig. 3. Computed variation of the bulk (a) Pd/Fe and (b) Ir/Fe ratio with the bulk Ni/Fe

ratio for metal grains that condense at equilibrium from a vaporized mixture of CR chondrite metal, H chondrite and residual nebular gas with a Ni/H enrichment of $1.4x10^4$ relative to solar composition and total pressure of 10^{-3} bar at a variety of Si/H enrichments. Theoretical curves are compared to the same measured data as in Fig. 1. Numbers and symbols as in Fig. 1.

Fig. 4. Curves showing the evolution of the calculated bulk composition (wt%) of the silicate fraction of the condensate in a plume produced by impact between a CR metal body and an H chondrite body at the indicated values of P^{tot} and Ni/H and Si/H enrichments relative to solar composition, compared to bulk analyses of BO and CC chondrules from CB_b chondrites (Krot *et al*. 2001a, b). Compositions are normalized to 100% ($CaO + Al_2O_3$) +MgO + SiO_2. Numbers on the curves are temperatures in K. Dashed portions of the curves are for temperature intervals where the SiO_2 content of the liquid calculated from the MELTS model differs from that predicted by the CMAS model by >2 wt% absolute, and the FeO content of the liquid <0.3 wt%. The curve for $P^{tot}=10^{-3}$ bar, Si/H=300xsolar and $Ni/H=1.4x10^3$xsolar is indistinguishable from the curve for the same P^{tot} and Si/H but with $Ni/H=1.4x10^4$xsolar. Grey diamond-Renazzo bulk silicate (Mason and Wiik, 1962); star-Bencubbin host silicate (Weisberg *et al*., 1990).

Fig. 5. Evolution of the calculated bulk composition (wt%) of the silicate fraction of the condensate in plumes produced by impact between a CR metal body and bodies with various differentiated silicate compositions at $P^{tot}=10^{-2}$ bar and Ni/H and Si/H enrichments of $1.4x10^3$ and 300, respectively, relative to solar composition. There was so little FeO in the aubrite case that the CMAS liquid model was used in the condensation calculation that resulted in the curve shown here. Numbers on the curves, symbols and

sources of chondrule analytical data as in Fig. 4.

Fig. 6. Computed variation of the bulk (a) Pd/Fe and (b) Ir/Fe ratio with the bulk Ni/Fe ratio for metal grains that condense at equilibrium from a vaporized mixture of CR core, residual nebular gas, and equal weight proportions of CR crust and residual CR mantle, having enrichments in Ni/H and Si/H of $3x10^4$ and 500, respectively, relative to solar composition for the total pressures shown. A second curve for 10^{-2} bar at a Ni/H enrichment of $3x10^3$ is also shown. When 20 wt% water is added to the total vaporized silicate, the positions of these curves are nearly unchanged. Curves labeled P/10 and P/1000 are bulk composition variations for zoned grains that condense from a gas with Ni/H and Si/H enrichments of $2.5x10^3$ and 500, respectively, when 20 wt% water is added to the total vaporized silicate, calculated using a kinetic model (see Section 3.4) at two different rates of decline of P^{tot} with temperature, *i.e.*, by factors of 10 and 10^3 over 500K. Theoretical curves are compared to the same measured data as in Fig. 1. Numbers and symbols as in Fig. 1.

Fig. 7. Curves showing the computed variation of Cr *vs* Ni contents of metal grains that condense from a vaporized mixture of CR core, CR residual mantle, CR crust, and residual nebular gas. The Si/H enrichment is 500 relative to solar composition in all cases, and the Ni/H enrichment is $3x10^4$ except in the 10^{-2} bar case in (a), where it is $3x10^3$. The weight proportions of CR crust to residual CR mantle are 1:1 in (a), but are variable in (b). Ni contents decrease with decreasing temperature. Also plotted for comparison are bulk compositions of unzoned metal grains in Bencubbin (Campbell et al., 2002) and zoned metal grains in QUE (Campbell et al., 2001). he latter calculated from traverses across the grains. Symbols as in Fig. 1.

Fig. 8. Evolution of oxygen fugacity relative to the iron-wüstite buffer (IW) as a function of temperature during condensation of a vaporized mixture of residual nebular gas, CR core and vaporized silicate that consists of equal proportions of residual CR mantle and CR crust at a P^{tot} of 10^{-3} bar and a Ni/H enrichment of $3x10^4$ relative to solar composition at Si/H enrichments of 300, 500 and $1.5x10^3$ relative to solar composition. Also shown are curves for the 300 and 500 Si/H cases when 15 and 20 wt% water, respectively, is added to the total vaporized silicates.

Fig. 9. Curves showing evolution of the calculated bulk composition (wt%) of the silicate fraction of the condensate in plumes produced by impact vaporization of a mixture of CR core, CR residual mantle, CR crust, residual nebular gas and, in some cases, water (a) normalized to 100% ($CaO + Al_2O_3$) + MgO + SiO_2, and (b) as wt% FeO *vs* wt% SiO_2. All cases shown are for $P^{tot}=10^{-3}$ bar and Si/H and Ni/H enrichments of 500 and $3x10^4$, respectively, relative to solar composition, except for one case in (b) at a Si/H enrichment of 1500. Curves are shown for the indicated weight ratios of vaporized mantle/total vaporized silicate. Solid curves labeled "No water" are those for plumes to which no water has been added, and broken curves labeled "20% water" are for plume compositions to which 20 g of water have been added for every 80 g of total silicate. Note that the evolutionary paths in (a) are very close to one another for a given mantle fraction whether or not water is added to the plume, but that the FeO content of the condensate in (b) is strongly dependent on the water abundance. BO chondrule compositions are best fit on (a) and (b) in plume regions where vaporized mantle composes 40-70 wt% of the total vaporized silicate. Calculated compositions of CR mantle and CR crust are shown by open and filled triangles, respectively. Numbers on

curves, sources of chondrule analytical data and other symbols as in Fig. 4. In (b), numbers in parentheses are mantle fractions.

Fig. 10. Curves showing the evolution of the calculated bulk composition (wt%) of the silicate fraction of the condensate in plumes produced by impact vaporization of a mixture of CR core, CR residual mantle, CR crust, residual nebular gas and water (a) normalized to 100% ($CaO + Al_2O_3$) + MgO + SiO_2, and (b) as wt% FeO *vs* wt% SiO_2, showing the effect of removal of the high-temperature condensate assemblage that forms at 2040K. All cases shown are for $P^{tot}=10^{-3}$ bar, Si/H and Ni/H enrichments of 500 and $3x10^4$, respectively, relative to solar composition, and CR mantle/total silicate and water/total silicate weight ratios of 0.4 and 0.25, respectively. Curves are shown for removal of the different fractions of the early condensate indicated. Note that BO chondrule compositions are best fit on both (a) and (b) at ~1820K after removal of 0-70% of the early condensate. Numbers, sources of chondrule analytical data and symbols as in Fig. 9.

Fig. 11. Curves showing the evolution of the calculated bulk composition (wt%) of the silicate fraction of the condensate in plumes produced by impact vaporization of a mixture of CR core, CR residual mantle, CR crust, residual nebular gas and, in some cases, water (a) normalized to 100% ($CaO + Al_2O_3$) + MgO + SiO_2, and (b) as wt% FeO *vs* wt% SiO_2. All cases shown are for $P^{tot}=10^{-3}$ bar and Si/H and Ni/H enrichments of 300 and $3x10^4$, respectively, relative to solar composition. Curves are shown for different weight ratios of vaporized mantle/total vaporized silicate. Broken curves labeled “15% water” are for plume compositions to which 15 g of water have been added for every 85 g of total silicate. Note that the evolutionary paths for a given mantle

fraction in (a) are very close to one another whether or not water is added to the plume, but the FeO content of the condensate is strongly dependent on the water abundance. CC chondrule compositions are best fit on (a) in plume regions where CR mantle ≥75 wt% of the total vaporized silicate. Labels, numbers, sources of chondrule analytical data and symbols as in Fig. 9.

Fig. 12. Curves showing the evolution of the calculated bulk composition (wt%) of the silicate fraction of the condensate in plumes produced by impact vaporization of a mixture of CR core, CR residual mantle, CR crust, residual nebular gas and water ice (a) normalized to 100% ($CaO + Al_2O_3$) + MgO + SiO_2, and (b) as wt% FeO *vs* wt% SiO_2, showing the effect of removal of the high-temperature condensate assemblage that forms at 1750K. All cases shown are for $P^{tot}=10^{-3}$ bar, Si/H and Ni/H enrichments of 300 and $3x10^4$, respectively, relative to solar composition, and CR mantle/total silicate and water/total silicate weight ratios of 0.4 and 0.176, respectively. Curves are shown for removal of the indicated fractions of the early condensate. Note that an early condensate assemblage with almost the same composition as the BO chondrule with the highest CaO + Al_2O_3 content is predicted to form at 1750K, and that the compositions of almost all CC chondrule compositions are best fit on both (a) and (b) at ~1710-1720K after removal of 95-100% of that early condensate. Numbers, sources of chondrule analytical data and symbols as in Fig. 9.

Fig. 13. Computed variation (curves with no data points) of CI chondrite-normalized (a) Ir/Fe, (b) Ni/Fe, (c) Co/Fe and (d) Cr/Fe ratios with distance from the center (most Ir-rich point) of a condensate metal alloy grain, compared to profiles measured by LA-ICP-MS across three metal grains in QUE (curves with data points). In the model, grain growth is

controlled by the kinetic theory of gases, as expressed by the Hertz-Knudsen equation. P^{tot} was assumed to be $1.6x10^{-4}$ bar at the metal nucleation temperature, and to fall by factors of ten (P/10) and one thousand (P/1000) over the next 500K. The gas was assumed to cool at 50K/hr, and to be supersaturated in siderophiles until the grain nucleated 101K (P/10) or 146K (P/1000) below the equilibrium condensation temperature of pure Ir. Continuous profiles predicted by theory were divided into 30 μm sections over which the compositions were averaged in order to match the spatial resolution of the analytical data. These averages are joined by line segments to generate the theoretical profiles on the plot.

Fig. 14. Computed variation of (a) δ^{56}Fe and (b) δ^{60}Ni with distance from the center of the same model condensate metal grains as in Fig. 13. The temperature interval for metal condensation is the same in both models, but the condensation rates are higher for the P/10 thermal history, resulting in more complete condensation, and a larger grain with less negative bulk δ^{56}Fe and δ^{60}Ni than in the P/1000 case. Continuous profiles predicted by theory were divided into 30 μm sections over which the compositions were averaged, as in Fig. 13.

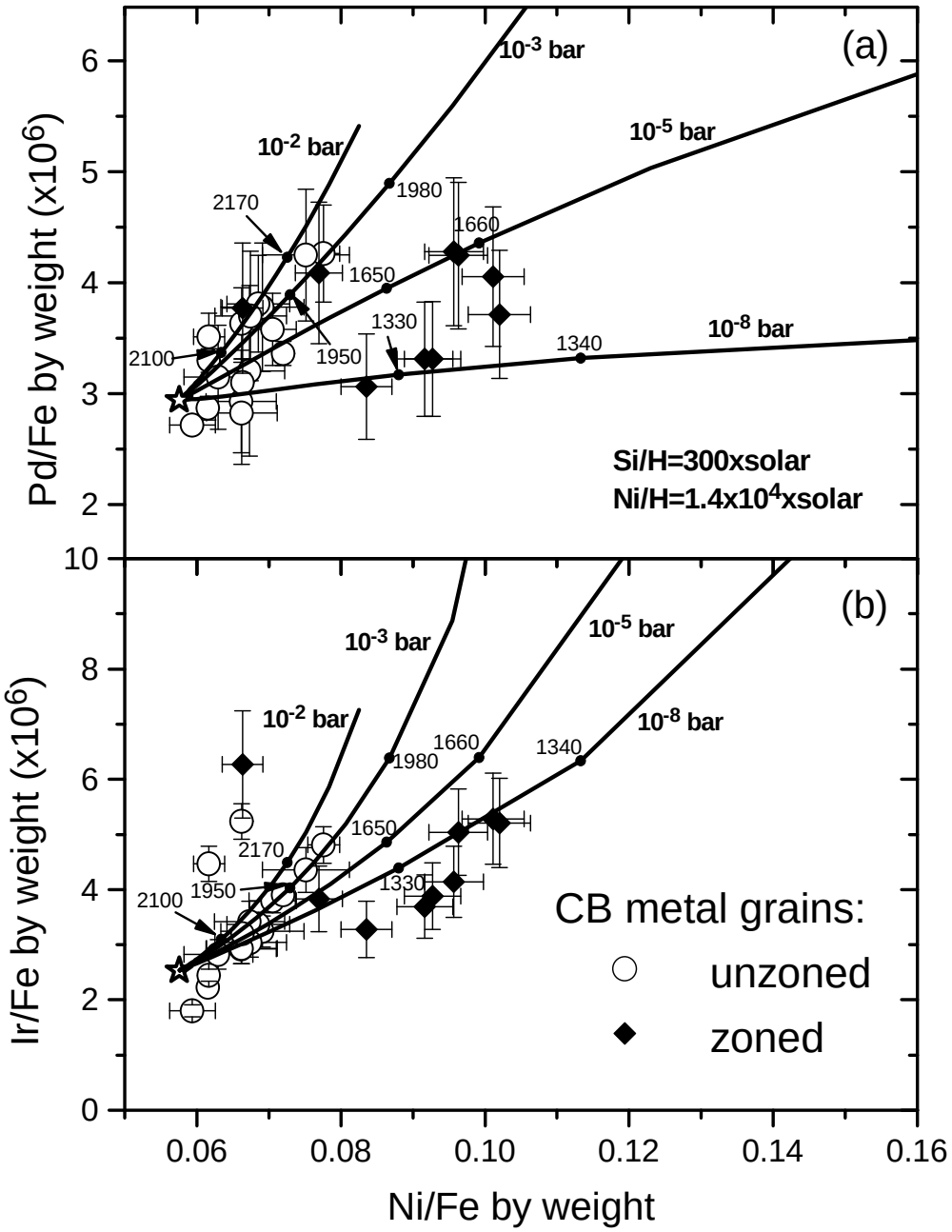
(a)
10-3 bar
10-2 bar
10-5 bar
10-8 bar
2170
1980
1660
1650
1330
1340
2100
1950
Si/H=300xsolar
Ni/H=1.4x10^4xsolar
Pd/Fe by weight (x10^6)
(b)
10-3 bar
10-5 bar
10-2 bar
10-8 bar
1660
1980
1340
1650
2170
1330
1950
2100
CB metal grains:
unzoned
zoned
Ir/Fe by weight (x10^6)
Ni/Fe by weight
0.06
0.08
0.10
0.12
0.14
0.16

Fig. 1

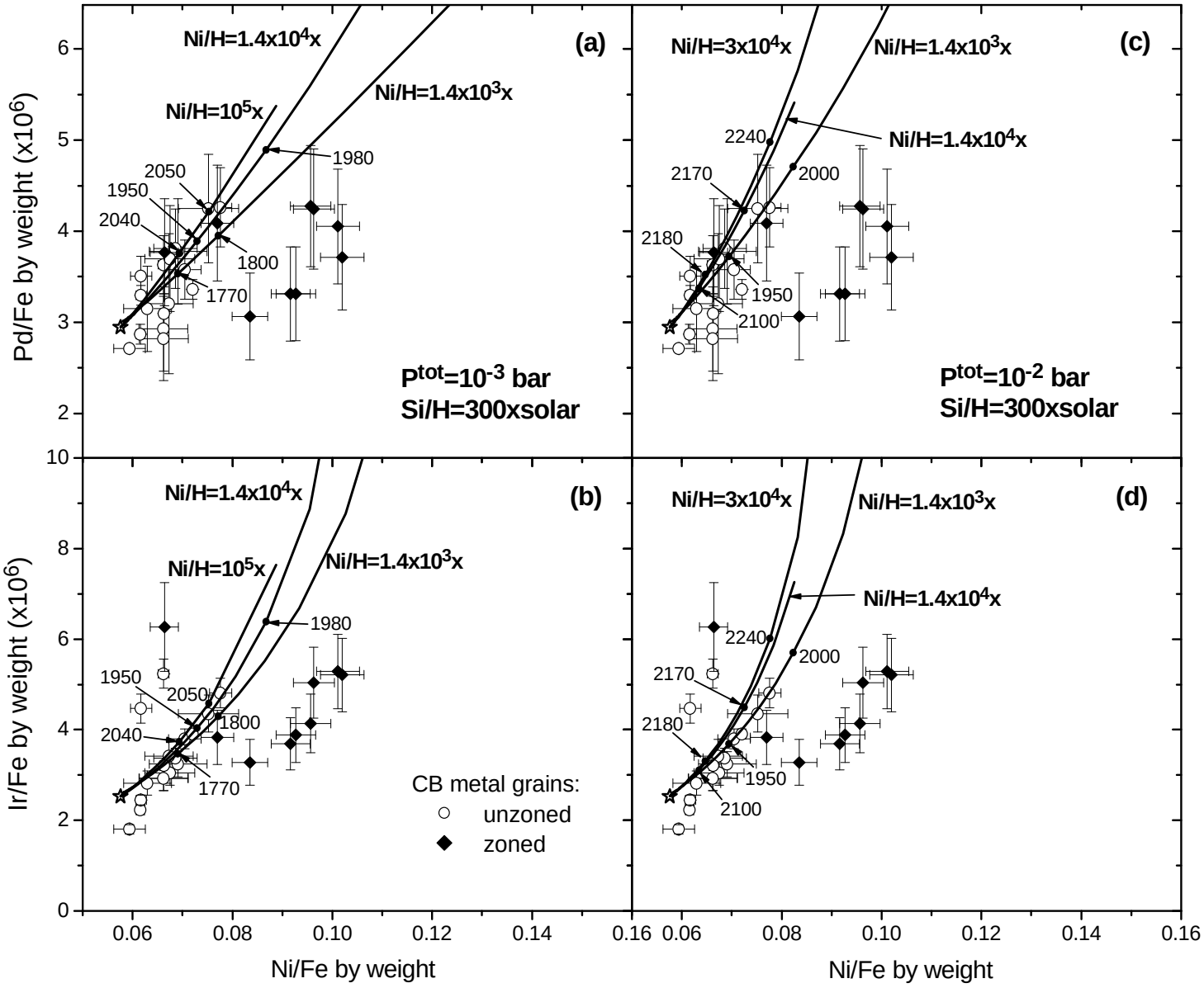
(a)
(b)
(c)
(d)
Ni/H=1.4x10^4x
Ni/H=10^5x
Ni/H=1.4x10^3x
Ni/H=3x10^4x
1980
2050
1950
2040
1800
1770
2240
2170
2000
2180
2100
P^tot=10^-3 bar
Si/H=300xsolar
P^tot=10^-2 bar
Si/H=300xsolar
Pd/Fe by weight (x10^6)
Ir/Fe by weight (x10^6)
Ni/Fe by weight
CB metal grains:
unzoned
zoned

Fig. 2

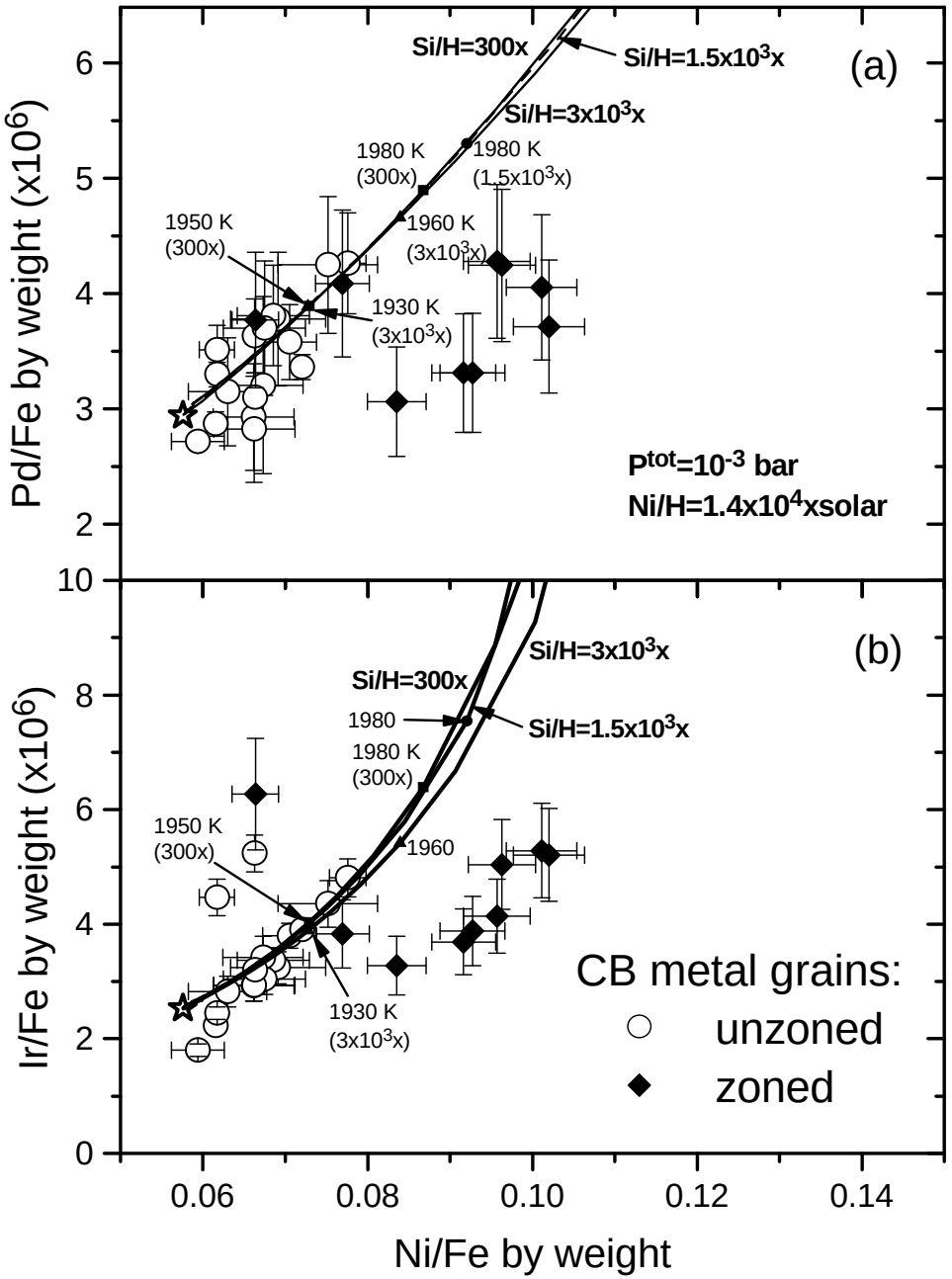
Si/H=300x
Si/H=1.5x10^{3}x
(a)
Si/H=3x10^{3}x
1980 K
(300x)
1980 K
(1.5x10^{3}x)
1950 K
(300x)
1960 K
(3x10^{3}x)
1930 K
(3x10^{3}x)
P^{tot}=10^{-3} bar
Ni/H=1.4x10^{4}xsolar
Pd/Fe by weight (x10^6)
Si/H=3x10^{3}x
(b)
Si/H=300x
1980
Si/H=1.5x10^{3}x
1980 K
(300x)
1950 K
(300x)
1960
1930 K
(3x10^{3}x)
CB metal grains:
unzoned
zoned
Ir/Fe by weight (x10^6)
Ni/Fe by weight

Fig. 3

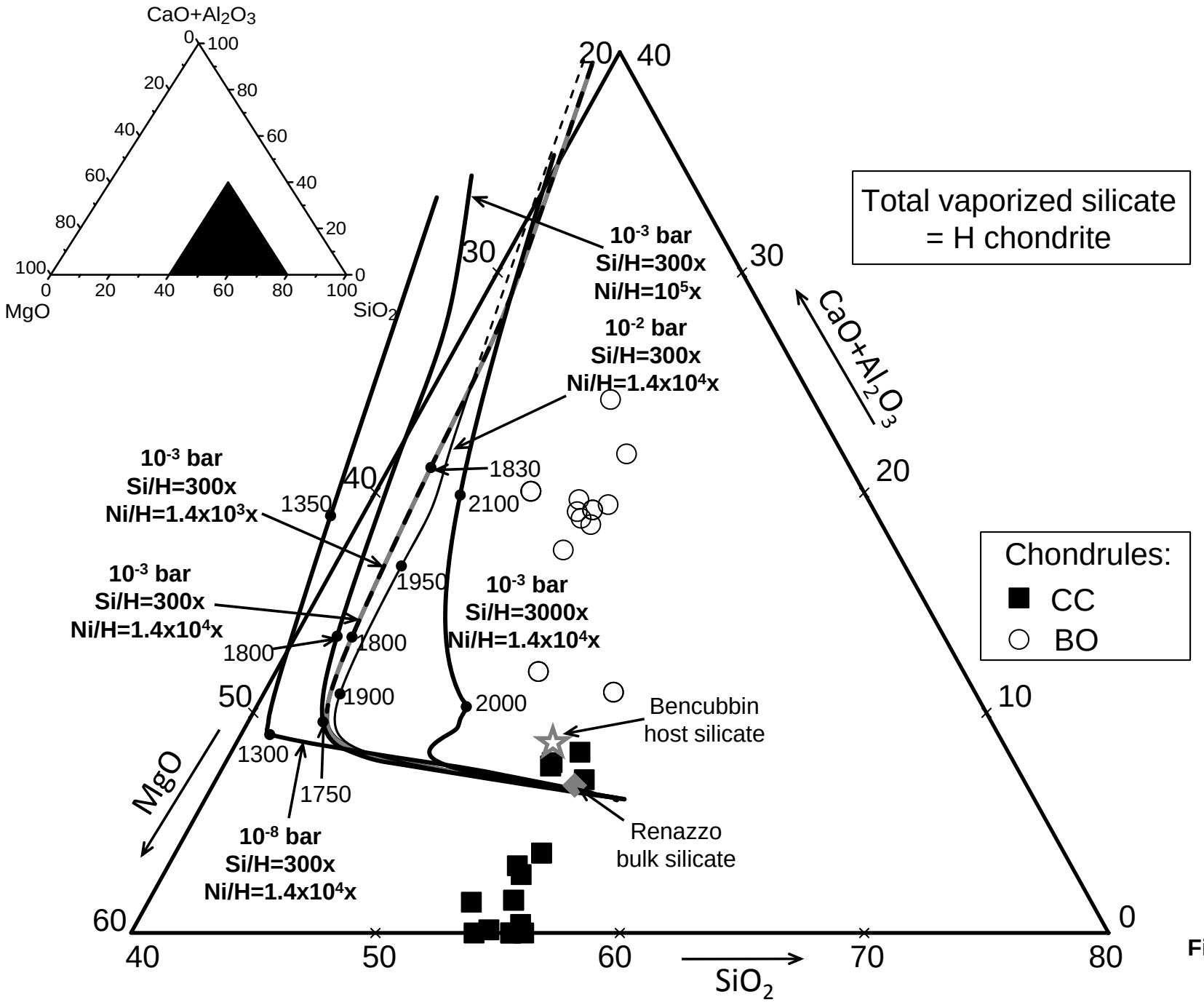
CaO+Al2O3
MgO
SiO2
Total vaporized silicate
= H chondrite
10-3 bar
Si/H=300x
Ni/H=10^5x
10-2 bar
Si/H=300x
Ni/H=1.4x10^4x
10-3 bar
Si/H=300x
Ni/H=1.4x10^3x
10-3 bar
Si/H=300x
Ni/H=1.4x10^4x
10-3 bar
Si/H=3000x
Ni/H=1.4x10^4x
10-8 bar
Si/H=300x
Ni/H=1.4x10^4x
1830
2100
1350
1950
1800
1800
1900
2000
1300
1750
Bencubbin
host silicate
Renazzo
bulk silicate
Chondrules:
CC
BO
CaO+Al2O3
MgO
SiO2

Fig. 4

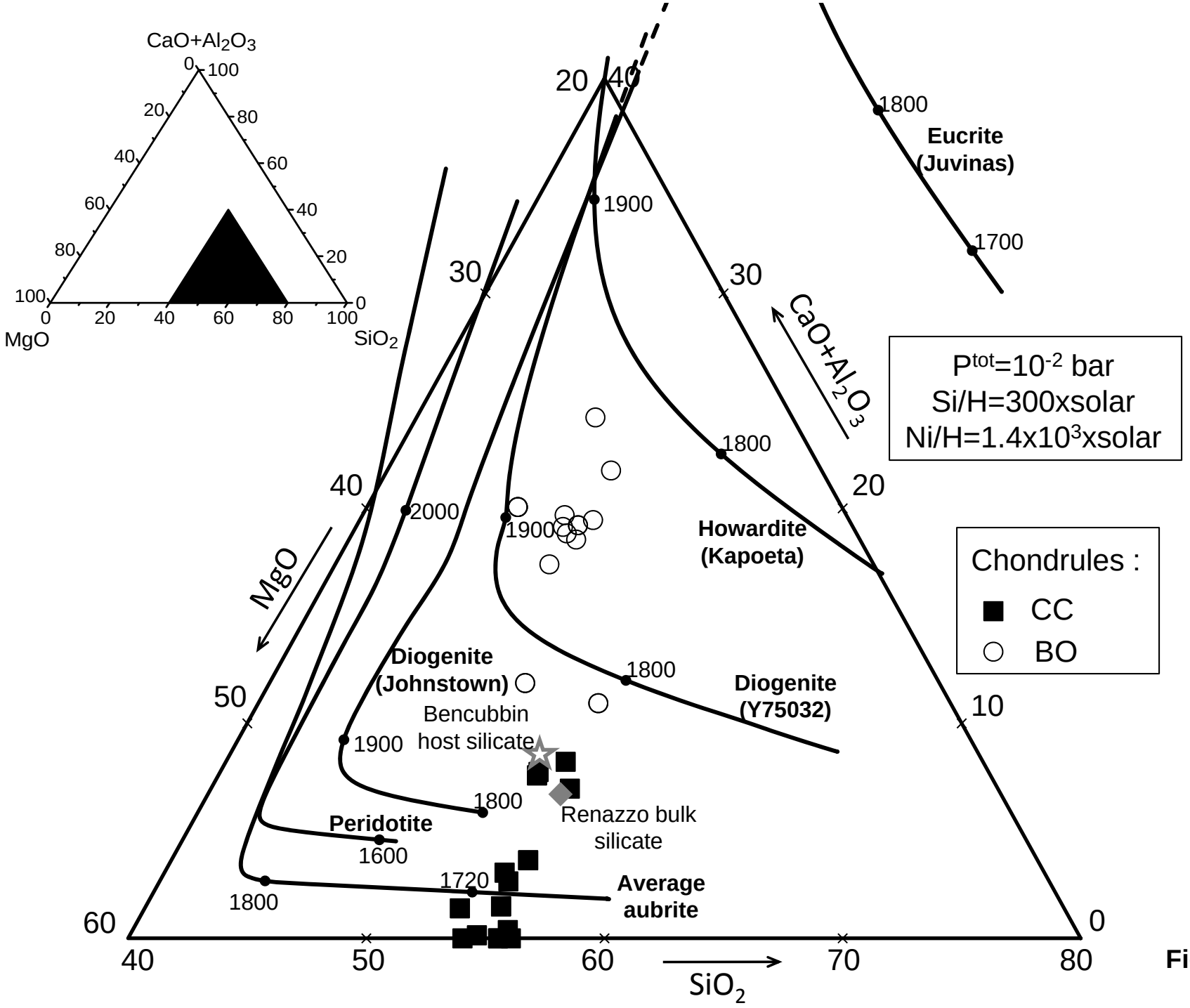
CaO+Al2O3
MgO
SiO2
Eucrite
(Juvinas)
1800
1700
1900
2000
Howardite
(Kapoeta)
Diogenite
(Johnstown)
Diogenite
(Y75032)
Bencubbin
host silicate
Renazzo bulk
silicate
Peridotite
1600
1720
Average
aubrite
P^tot=10^-2 bar
Si/H=300xsolar
Ni/H=1.4x10^3xsolar
Chondrules :
CC
BO
MgO
CaO+Al2O3
SiO2

Fig. 5

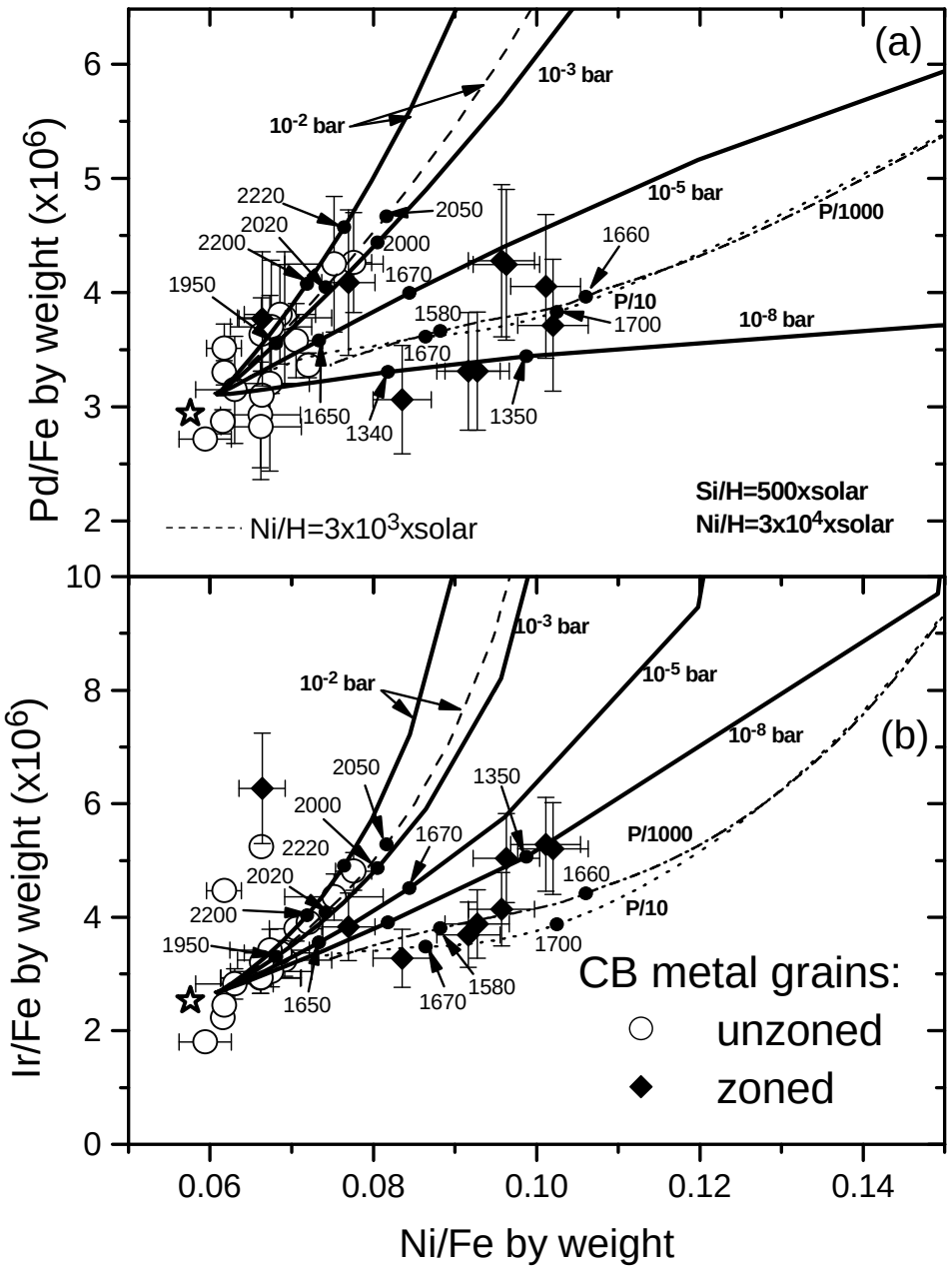
(a)
Pd/Fe by weight (x10^6)
10^-2 bar
10^-3 bar
10^-5 bar
10^-8 bar
P/1000
P/10
2220
2050
2020
2200
2000
1660
1670
1950
1580
1700
1670
1650
1340
1350
Si/H=500xsolar
Ni/H=3x10^4xsolar
Ni/H=3x10^3xsolar
(b)
Ir/Fe by weight (x10^6)
10^-3 bar
10^-2 bar
10^-5 bar
10^-8 bar
2050
1350
2000
1670
P/1000
2220
2020
1660
P/10
2200
1950
1700
1650
1670
1580
CB metal grains:
unzoned
zoned
0.06
0.08
0.10
0.12
0.14
Ni/Fe by weight

Fig.6

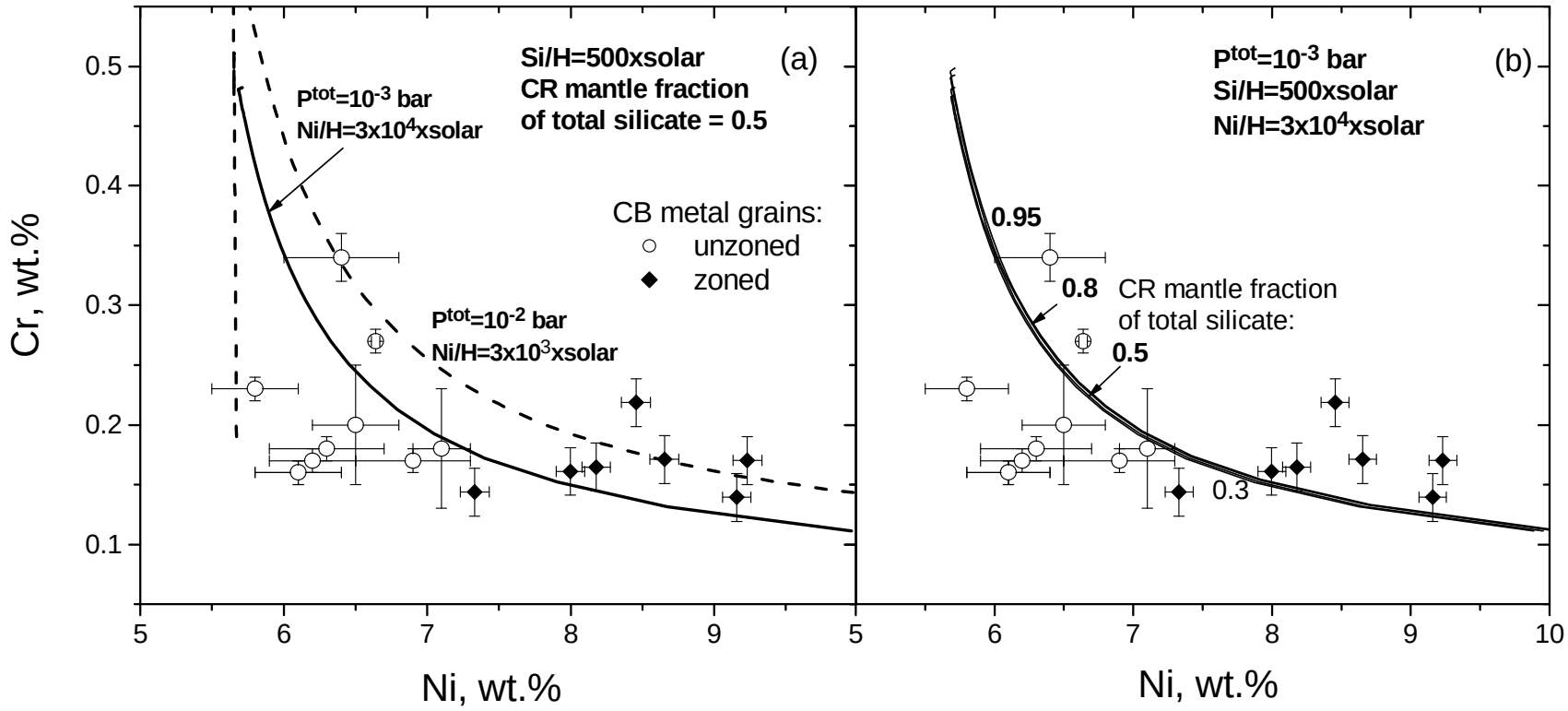
Si/H=500xsolar
CR mantle fraction
of total silicate = 0.5
(a)
P^tot=10^-3 bar
Ni/H=3x10^4xsolar
P^tot=10^-2 bar
Ni/H=3x10^3xsolar
CB metal grains:
unzoned
zoned
Cr, wt.%
Ni, wt.%
P^tot=10^-3 bar
Si/H=500xsolar
Ni/H=3x10^4xsolar
(b)
0.95
0.8
0.5
0.3
CR mantle fraction
of total silicate:
Ni, wt.%

Fig. 7

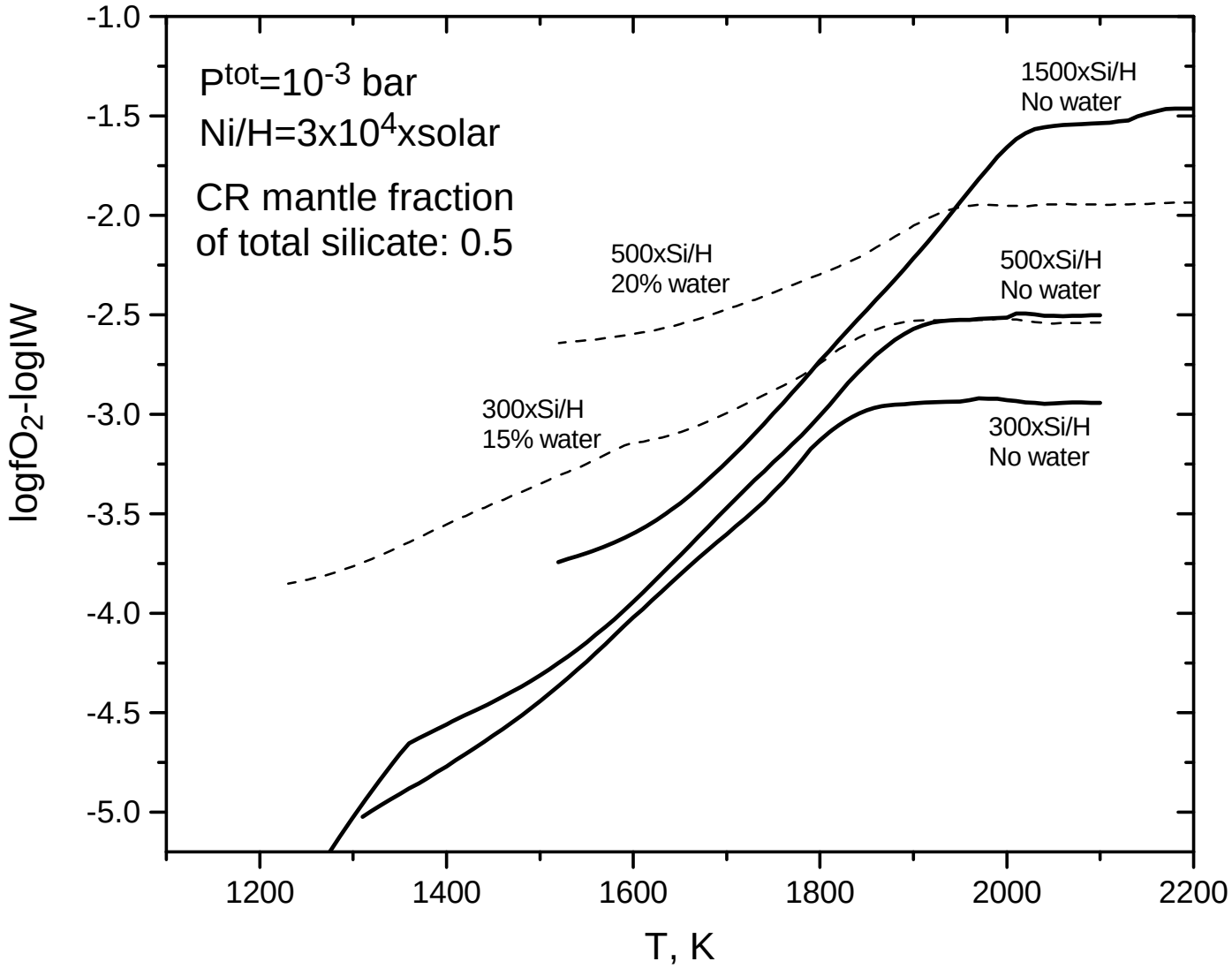
$P^{tot}=10^{-3}$ bar
$Ni/H=3x10^{4}$xsolar
CR mantle fraction
of total silicate: 0.5
1500xSi/H
No water
500xSi/H
20% water
500xSi/H
No water
300xSi/H
15% water
300xSi/H
No water
$logfO_2$-logIW
T, K
-1.0
-1.5
-2.0
-2.5
-3.0
-3.5
-4.0
-4.5
-5.0
1200
1400
1600
1800
2000
2200

Fig. 8

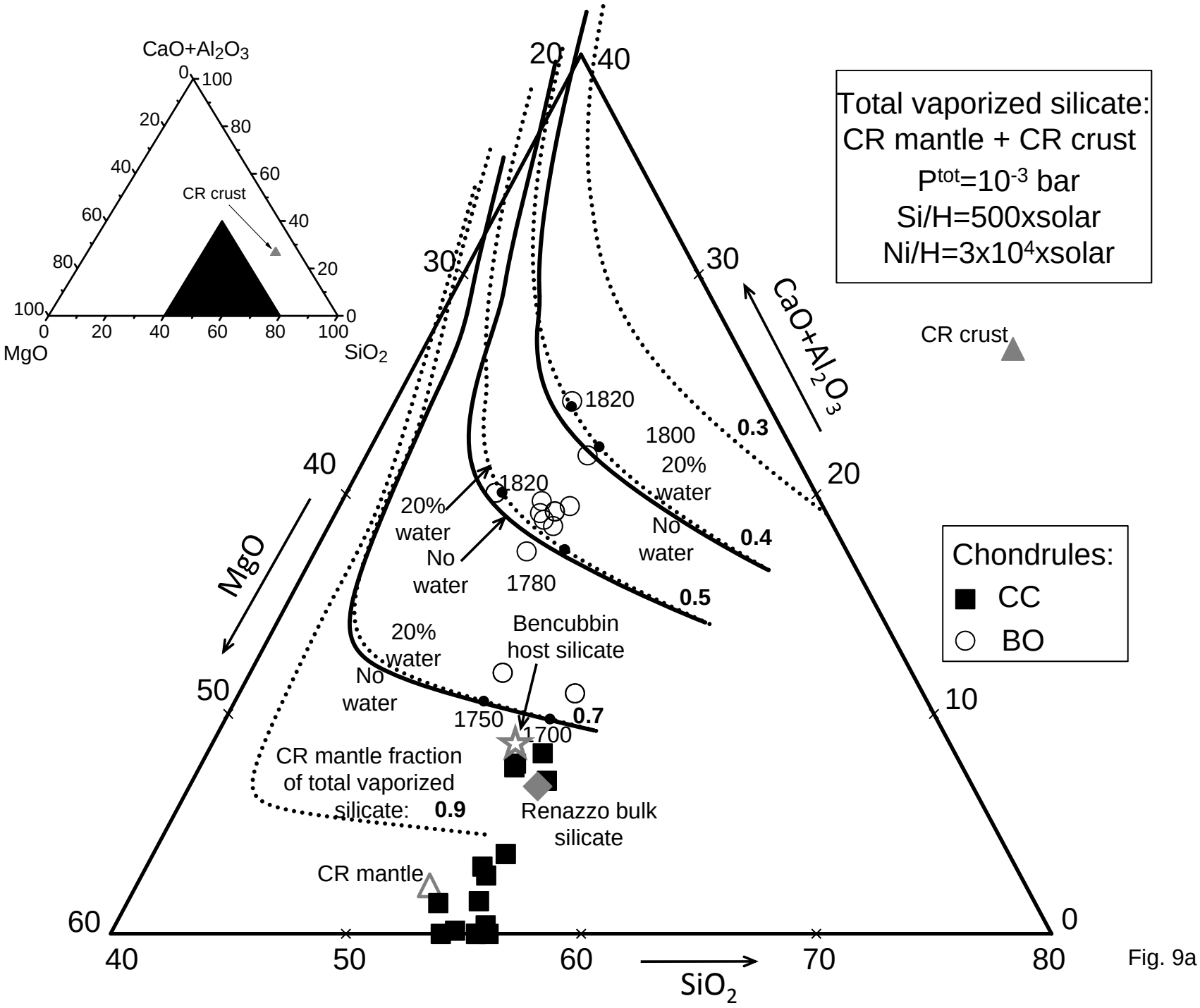
CaO+Al2O3
MgO
SiO2
CR crust
Total vaporized silicate:
CR mantle + CR crust
Ptot=10-3 bar
Si/H=500xsolar
Ni/H=3x10⁴xsolar
CR crust
CaO+Al2O3
1820
1800
20%
water
No
water
0.3
0.4
0.5
0.7
1820
20%
water
No
water
1780
20%
water
No
water
Bencubbin
host silicate
1750
1700
Chondrules:
CC
BO
CR mantle fraction
of total vaporized
silicate: 0.9
Renazzo bulk
silicate
CR mantle
MgO
SiO2

Fig. 9a

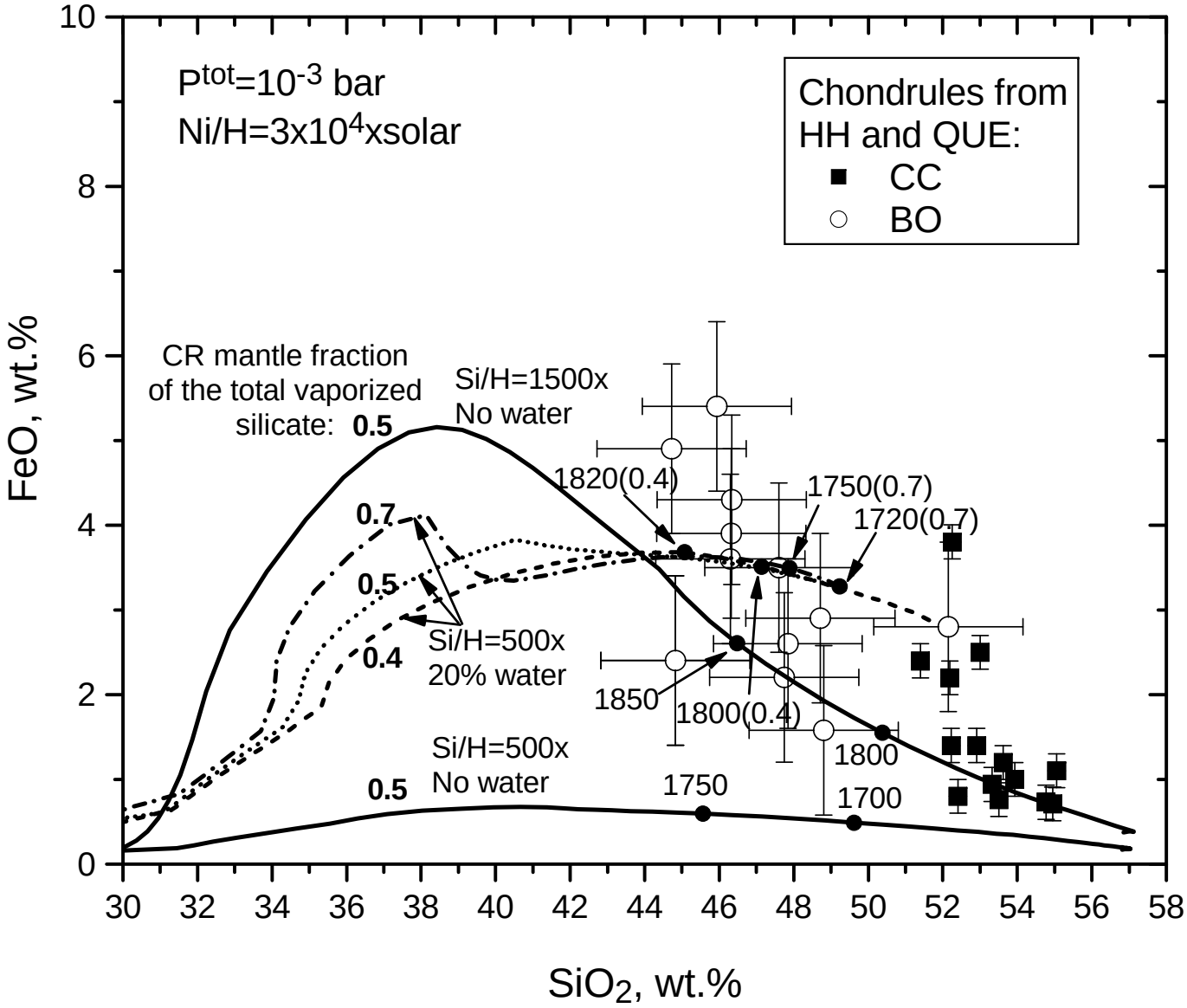
P^tot=10^-3 bar
Ni/H=3x10^4xsolar
Chondrules from HH and QUE:
CC
BO
CR mantle fraction of the total vaporized silicate:
0.5
0.7
0.5
0.4
0.5
Si/H=1500x
No water
Si/H=500x
20% water
Si/H=500x
No water
1820(0.4)
1750(0.7)
1720(0.7)
1850
1800(0.4)
1800
1750
1700
FeO, wt.%
SiO2, wt.%
0
2
4
6
8
10
30
32
34
36
38
40
42
44
46
48
50
52
54
56
58

Fig. 9b

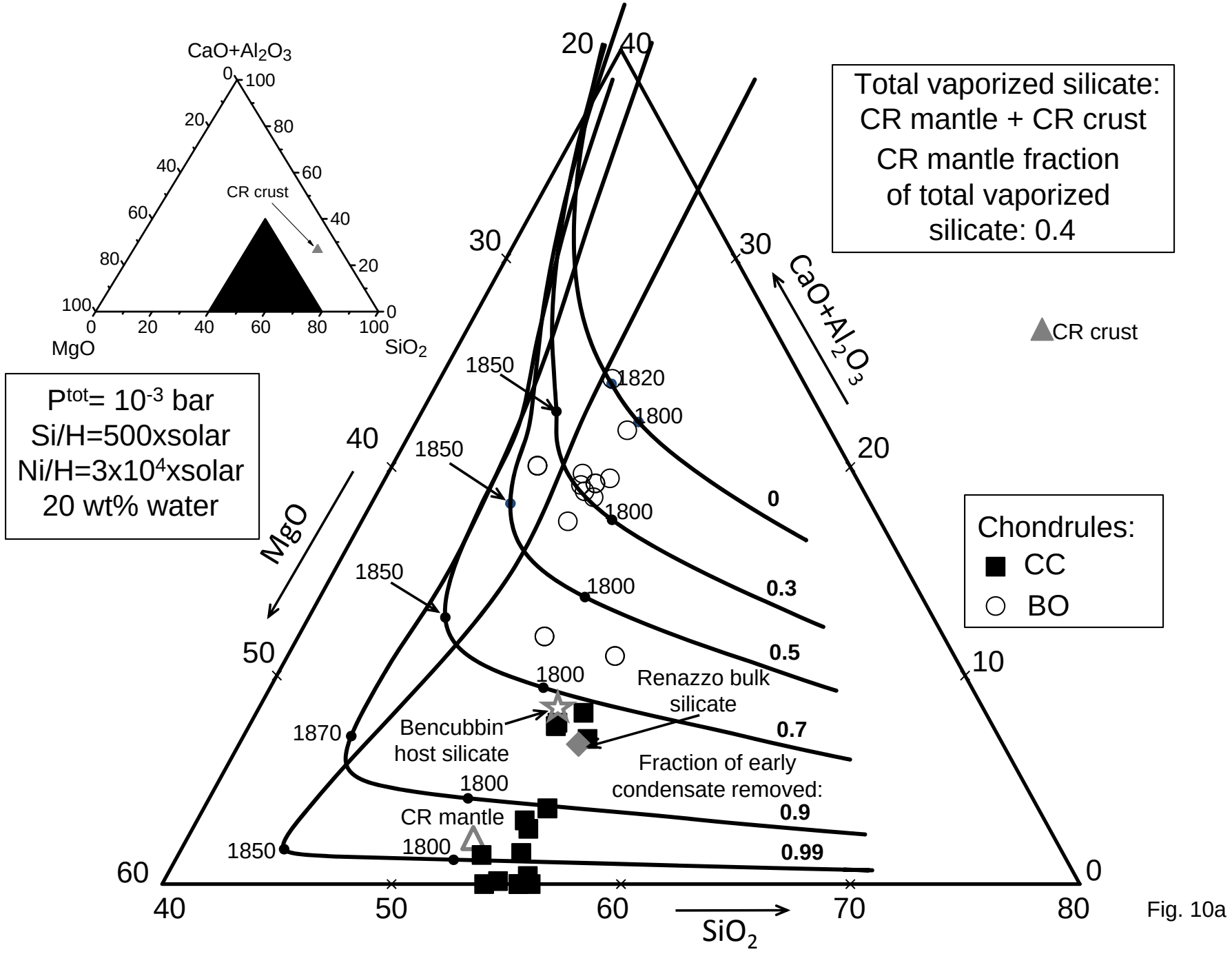
CaO+Al2O3
MgO
SiO2
CR crust
Total vaporized silicate:
CR mantle + CR crust
CR mantle fraction
of total vaporized
silicate: 0.4
Ptot= 10-3 bar
Si/H=500xsolar
Ni/H=3x10⁴xsolar
20 wt% water
Chondrules:
CC
BO
Renazzo bulk
silicate
Bencubbin
host silicate
CR mantle
Fraction of early
condensate removed:
0
0.3
0.5
0.7
0.9
0.99
1850
1820
1800
1870

Fig. 10a

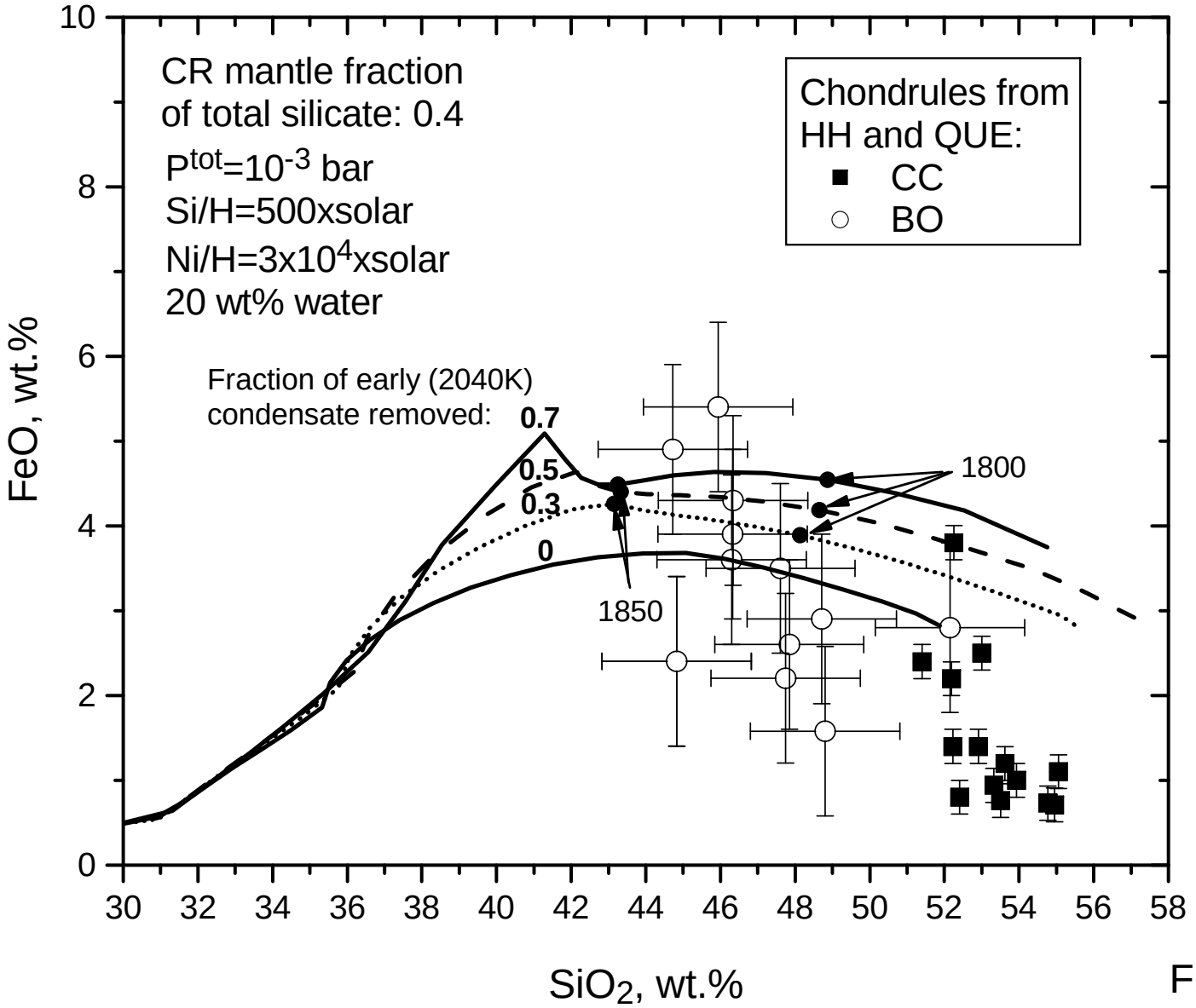
CR mantle fraction
of total silicate: 0.4
P^tot=10^-3 bar
Si/H=500xsolar
Ni/H=3x10^4xsolar
20 wt% water
Chondrules from
HH and QUE:
CC
BO
Fraction of early (2040K)
condensate removed:
0.7
0.5
0.3
0
1800
1850
FeO, wt.%
SiO2, wt.%
0
2
4
6
8
10
30
32
34
36
38
40
42
44
46
48
50
52
54
56
58

Fig. 10b

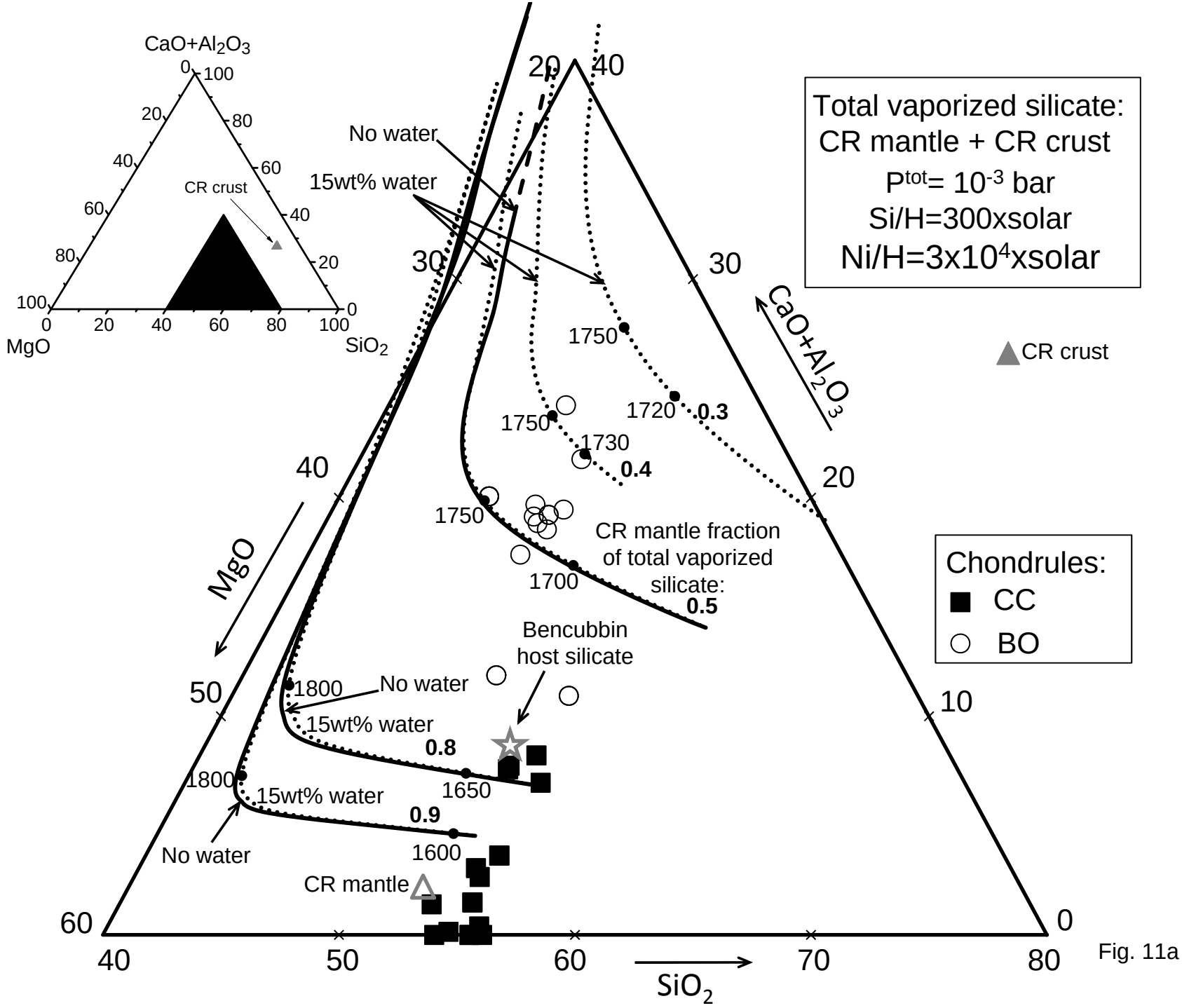
CaO+Al2O3
MgO
SiO2
CR crust
Total vaporized silicate:
CR mantle + CR crust
Ptot= 10-3 bar
Si/H=300xsolar
Ni/H=3x10⁴xsolar
No water
15wt% water
CaO+Al2O3
MgO
SiO2
CR crust
1750
1720
0.3
1730
0.4
1750
1750
CR mantle fraction
of total vaporized
silicate:
1700
0.5
Chondrules:
CC
BO
Bencubbin
host silicate
1800
No water
15wt% water
0.8
1650
1800
15wt% water
0.9
No water
1600
CR mantle

Fig. 11a

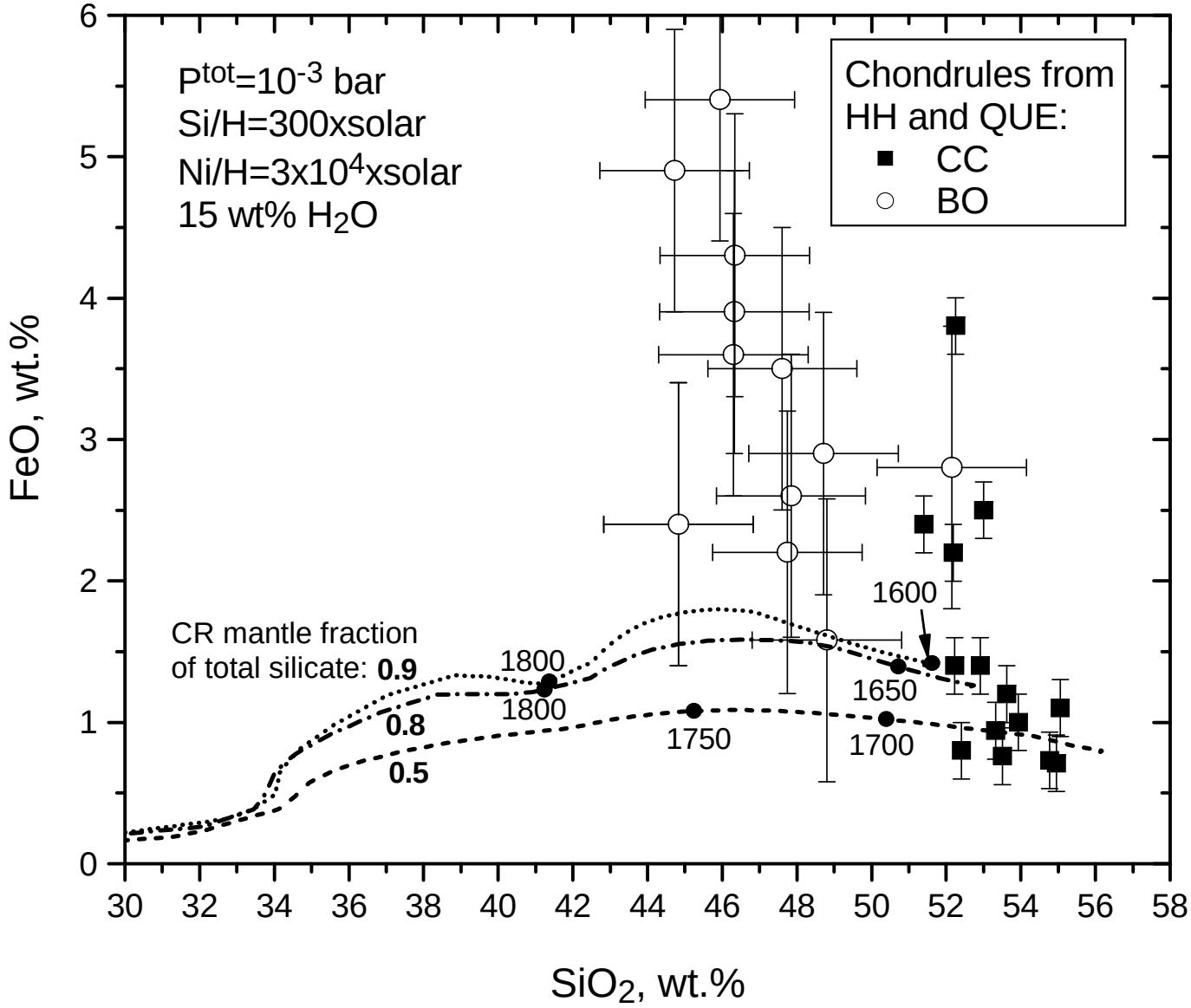
P^tot=10^-3 bar
Si/H=300xsolar
Ni/H=3x10^4xsolar
15 wt% H2O
Chondrules from HH and QUE:
CC
BO
CR mantle fraction of total silicate: 0.9
0.8
0.5
1800
1800
1750
1700
1650
1600
FeO, wt.%
SiO2, wt.%
0
1
2
3
4
5
6
30
32
34
36
38
40
42
44
46
48
50
52
54
56
58

Fig. 11b

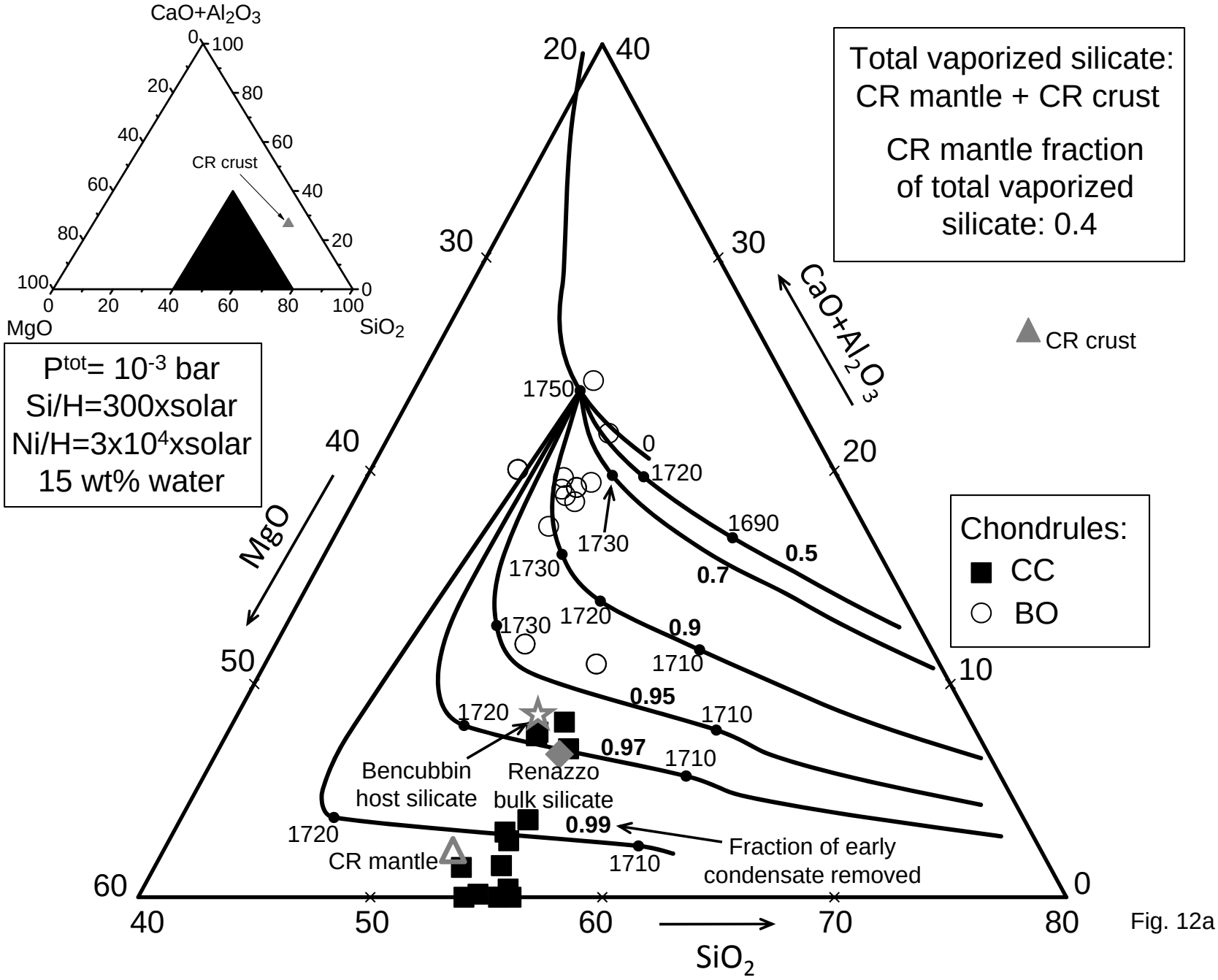
CaO+Al2O3
MgO
SiO2
CR crust
Total vaporized silicate:
CR mantle + CR crust
CR mantle fraction
of total vaporized
silicate: 0.4
CR crust
P^tot= 10^-3 bar
Si/H=300xsolar
Ni/H=3x10^4xsolar
15 wt% water
Chondrules:
CC
BO
1750
1720
1690
1730
1710
0
0.5
0.7
0.9
0.95
0.97
0.99
Bencubbin
host silicate
Renazzo
bulk silicate
CR mantle
Fraction of early
condensate removed
SiO2

Fig. 12a

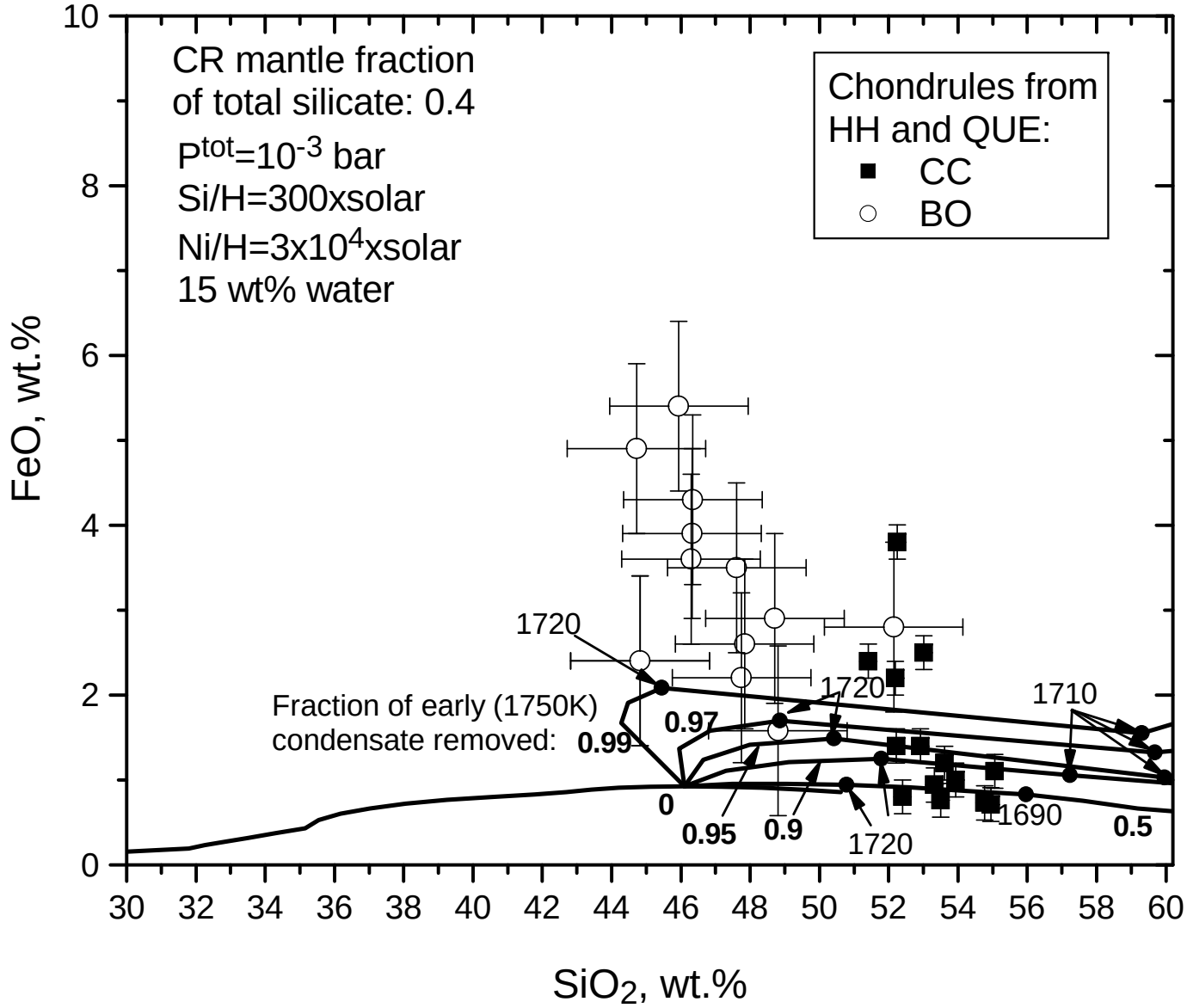
CR mantle fraction
of total silicate: 0.4
P^tot=10^-3 bar
Si/H=300xsolar
Ni/H=3x10^4xsolar
15 wt% water
Chondrules from
HH and QUE:
CC
BO
FeO, wt.%
SiO2, wt.%
Fraction of early (1750K)
condensate removed:
0.99
0.97
0
0.95
0.9
0.5
1720
1720
1720
1710
1690

Fig. 12b

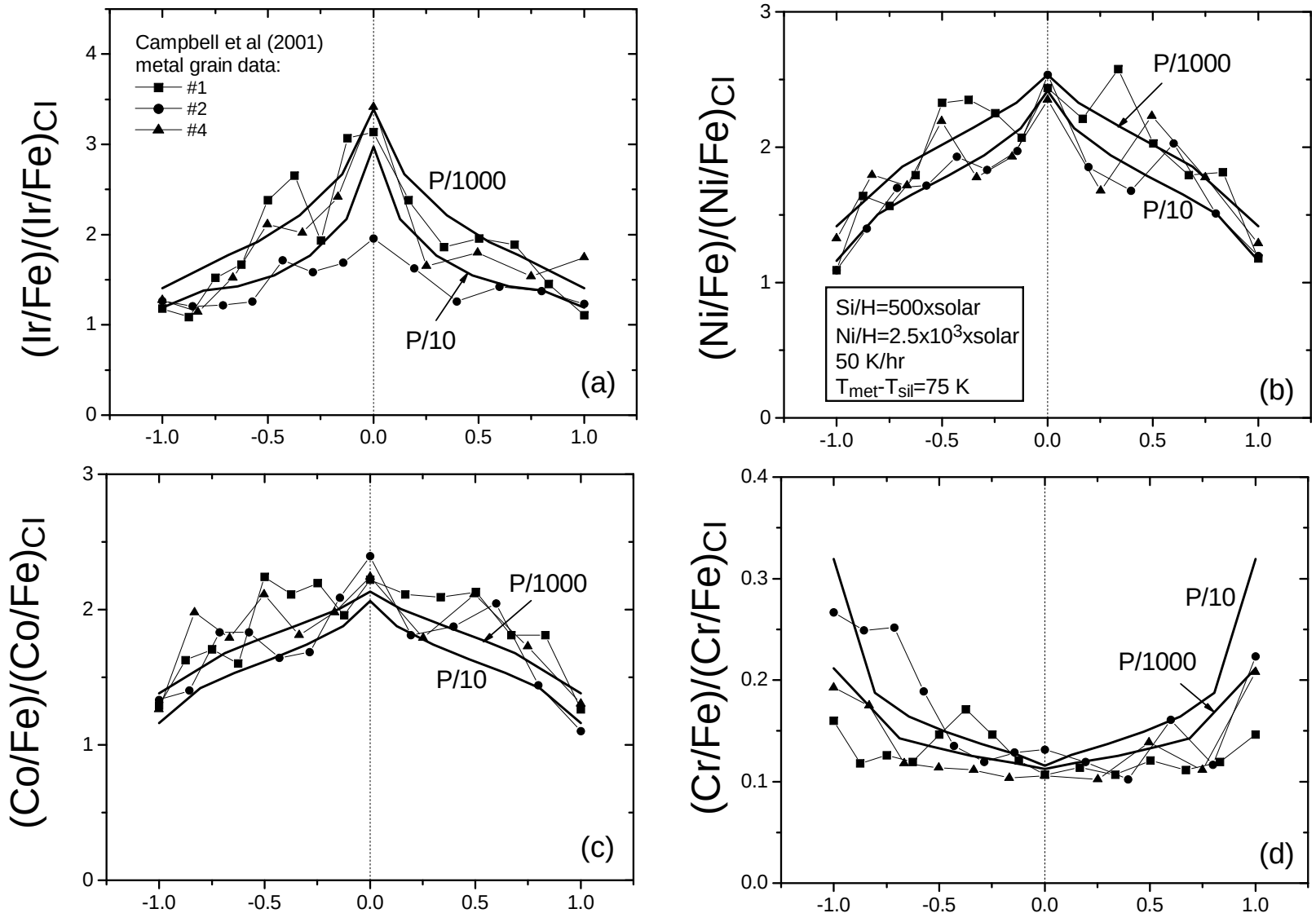
Campbell et al (2001)
metal grain data:
#1
#2
#4
P/1000
P/10
(a)
(Ir/Fe)/(Ir/Fe)CI
P/1000
P/10
Si/H=500xsolar
Ni/H=2.5x10^3xsolar
50 K/hr
Tmet-Tsil=75 K
(b)
(Ni/Fe)/(Ni/Fe)CI
P/1000
P/10
(c)
(Co/Fe)/(Co/Fe)CI
P/10
P/1000
(d)
(Cr/Fe)/(Cr/Fe)CI
Fractional radius of the metal grain

Fig. 13

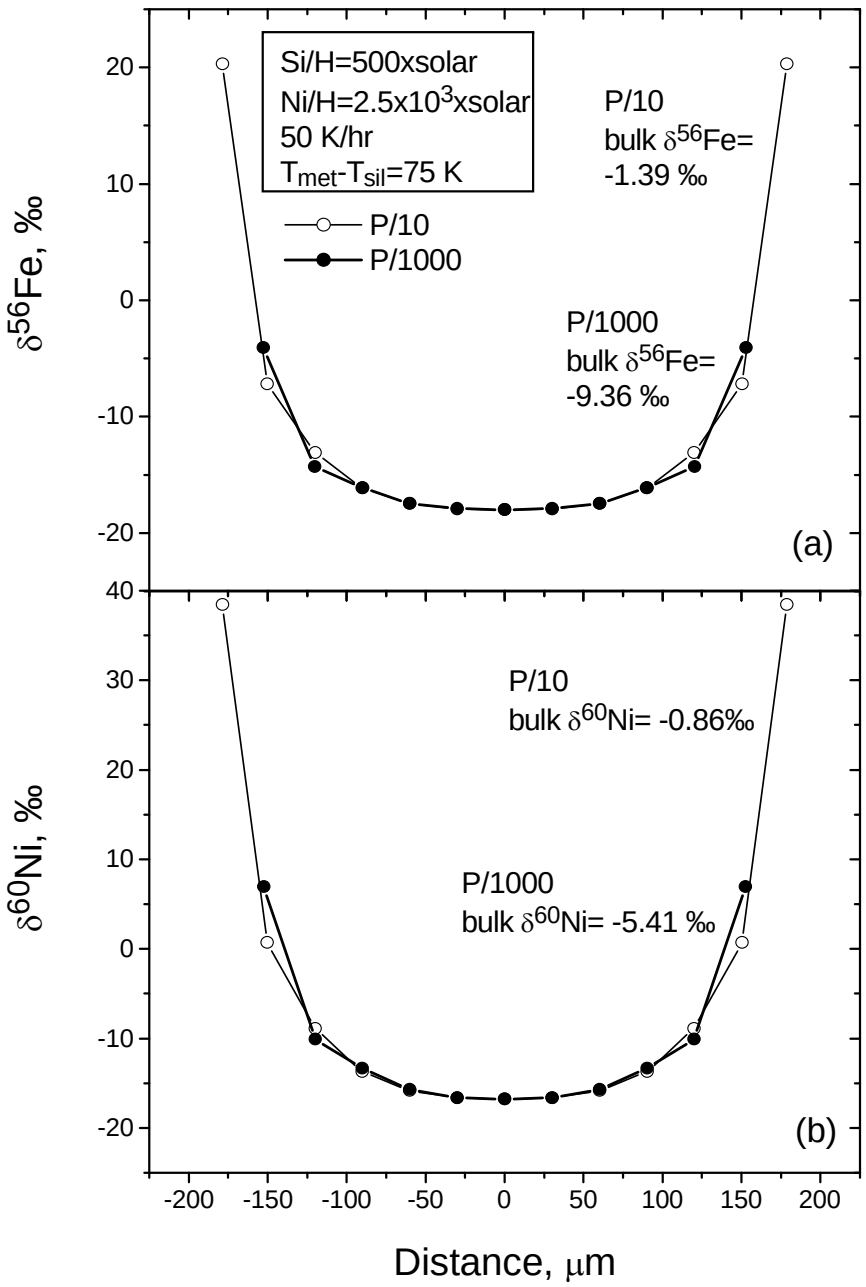
Si/H=500xsolar
Ni/H=2.5x10^3xsolar
50 K/hr
T_met-T_sil=75 K
P/10
P/1000
P/10
bulk δ56Fe=
-1.39 ‰
P/1000
bulk δ56Fe=
-9.36 ‰
(a)
P/10
bulk δ60Ni= -0.86‰
P/1000
bulk δ60Ni= -5.41 ‰
(b)
δ56Fe, ‰
δ60Ni, ‰
Distance, μm

Fig. 14

Table 1. Relative atomic abundances of components used in this work.

1 Element	2 Average H chondrite[1]	3 Residual nebular gas[2]	4 CR chondrite metal[3]	5 Model plume composition[4]
H	8.026E+04	2.790E+10	-	9.308E+07
He	0.000E+00	2.720E+09	-	9.067E+06
C	1.503E+04	6.834E+06	-	3.781E+04
N	0.000E+00	3.130E+06	-	1.043E+04
O	3.455E+06	1.021E+07	-	3.489E+06
Na	4.470E+04	1.270E+04	-	4.474E+04
Mg	9.591E+05	1.149E+05	-	9.595E+05
Al	6.936E+04	1.554E+04	-	6.941E+04
Si	1.000E+06	0.000E+00	-	1.000E+06
P	6.245E+03	4.155E+03	-	6.259E+03
S	1.002E+05	3.456E+05	-	1.013E+05
K	3.283E+03	4.866E+02	-	3.285E+03
Ca	5.079E+04	1.031E+04	-	5.082E+04
Ti	2.466E+03	0.000E+00	-	2.466E+03
Cr	1.159E+04	1.913E+03	2.627E+03	1.324E+05
Mn	6.933E+03	2.617E+03	-	6.941E+03
Fe	7.966E+05	1.034E+05	9.000E+05	4.219E+07
Co	2.315E+03	0.000E+00	2.250E+03	1.058E+05
Ni	4.558E+04	3.722E+03	4.930E+04	2.313E+06
Pd	1.374E+00	1.553E-02	1.390E+00	6.530E+01
Ir	6.756E-01	0.000E+00	6.610E-01	3.108E+01

[1]Si, Ti, C, H, O, P and S are from Jarosewich (1990); others from Kallemeyn et al. (1989); Pd from average H chondrite Pd/Ir of Horan et al. (2003), in atoms/10^6 Si

[2]After removal of average H chondrite

[3]Kong et al. (1999) average CR metal but Ir/Ni and Pd/Ni were assumed to be solar (Anders and Grevesse, 1989)

[4]89.3 wt% CR metal + 6.0 wt% H chondrite + 4.7 wt% of residual nebular gas to yield Ni/H=1.4x10^4 and Si/H=300 times their solar values, respectively, in atoms/10^6 Si

Table 2. Atomic abundances of differentiated silicate components used in this work, relative to 10^6 Si, and of plumes made from them that are enriched in Ni/H and Si/H by factors of 1.4×10^3 and 300.

	Average aubrite		Juvinas		Kapoeta		Y75032		Johnstown		Peridotite	
	Pure component	Model plume composition[1]	Pure component	Model plume composition[2]	Pure component	Model plume composition[3]	Pure component	Model plume composition[4]	Pure component	Model plume composition[5]	Pure component	Model plume composition[6]
H	0.000E+00	9.300E+07	0.000E+00	9.300E+07	0.000E+00	9.300E+07	0.000E+00	9.300E+07	0.000E+00	9.300E+07	0.000E+00	9.300E+07
He	0.000E+00	9.067E+06	0.000E+00	9.067E+06	0.000E+00	9.067E+06	0.000E+00	9.067E+06	0.000E+00	9.067E+06	0.000E+00	9.067E+06
C	0.000E+00	2.278E+04	0.000E+00	2.278E+04	0.000E+00	2.278E+04	0.000E+00	2.278E+04	0.000E+00	2.278E+04	0.000E+00	2.278E+04
N	0.000E+00	1.043E+04	0.000E+00	1.043E+04	0.000E+00	1.043E+04	0.000E+00	1.043E+04	0.000E+00	1.043E+04	0.000E+00	1.043E+04
O	3.016E+06	3.050E+06	3.268E+06	3.302E+06	3.201E+06	3.235E+06	3.104E+06	3.138E+06	3.095E+06	3.129E+06	3.719E+06	3.753E+06
Na	6.732E+03	6.774E+03	1.486E+04	1.490E+04	1.064E+04	1.068E+04	3.665E+03	3.707E+03	7.386E+02	7.809E+02	2.172E+03	2.214E+03
Mg	9.654E+05	9.658E+05	2.000E+05	2.004E+05	4.683E+05	4.687E+05	5.890E+05	5.894E+05	7.241E+05	7.245E+05	1.415E+06	1.415E+06
Al	1.862E+04	1.867E+04	3.114E+05	3.115E+05	1.945E+05	1.945E+05	7.575E+04	7.580E+04	3.367E+04	3.373E+04	5.967E+04	5.972E+04
Si	1.000E+06	1.000E+06	1.000E+06	1.000E+06	1.000E+06	1.000E+06	1.000E+06	1.000E+06	1.000E+06	1.000E+06	1.000E+06	1.000E+06
P	0.000E+00	1.385E+01	0.000E+00	1.385E+01	0.000E+00	1.385E+01	0.000E+00	1.385E+01	0.000E+00	1.385E+01	0.000E+00	1.385E+01
S	1.590E+04	1.705E+04	0.000E+00	1.152E+03	0.000E+00	1.152E+03	0.000E+00	1.152E+03	2.864E+03	9.006E+03	0.000E+00	1.152E+03
K	6.644E+02	6.660E+02	7.000E+02	7.017E+02	5.579E+02	5.596E+02	1.688E+02	1.704E+02	2.673E+01	2.835E+01	0.000E+00	1.622E+00
Ca	1.581E+04	1.585E+04	2.395E+05	2.396E+05	1.108E+05	1.108E+05	7.312E+04	7.315E+04	3.735E+04	3.738E+04	4.440E+04	4.444E+04
Ti	6.528E+02	6.528E+02	9.629E+03	9.629E+03	4.485E+03	4.485E+03	3.696E+03	3.696E+03	1.432E+03	1.432E+03	5.054E+02	5.054E+02
Cr	4.118E+02	1.262E+04	4.901E+03	1.714E+04	1.091E+04	2.311E+04	1.031E+04	2.246E+04	1.235E+04	2.460E+04	8.679E+03	2.092E+04
Mn	5.882E+02	5.969E+02	8.866E+03	8.875E+03	8.335E+03	8.344E+03	9.767E+03	9.776E+03	7.809E+03	7.817E+03	0.000E+00	8.725E+00
Fe	7.669E+04	4.258E+06	3.179E+05	4.509E+06	2.910E+05	4.470E+06	2.940E+05	4.452E+06	2.561E+05	4.447E+06	1.549E+05	4.348E+06
Co	0.000E+00	1.045E+04	0.000E+00	1.048E+04	0.000E+00	1.045E+04	0.000E+00	1.040E+04	0.000E+00	1.048E+04	0.000E+00	1.048E+04
Ni	1.066E+03	2.301E+05	0.000E+00	2.296E+05	0.000E+00	2.289E+05	0.000E+00	2.278E+05	0.000E+00	2.297E+05	0.000E+00	2.297E+05
Pd	0.000E+00	6.457E+00	0.000E+00	6.473E+00	0.000E+00	6.454E+00	0.000E+00	6.422E+00	0.000E+00	6.477E+00	0.000E+00	6.475E+00
Ir	0.000E+00	3.071E+00	0.000E+00	3.078E+00	0.000E+00	5.115E+00	0.000E+00	3.054E+00	0.000E+00	3.080E+00	0.000E+00	3.079E+00

[1]51.1 wt% CR metal + 21.9 wt% average aubrite + 27 wt% of residual nebular gas.

[2]49.5 wt% CR metal + 24.4 wt% Juvinas + 26.1 wt% of residual nebular gas.

[3]49.9 wt% CR metal + 23.8 wt% Kapoeta + 26.4 wt% of residual nebular gas.

[4]50.1 wt% CR metal + 23.3 wt% Y75032 + 26.6 wt% of residual nebular gas.

[5]50.5 wt% CR metal + 23 wt% Johnstown + 26.5 wt% of residual nebular gas.

[6]48.4 wt% CR metal + 26.1 wt% peridotite + 25.5 wt% of residual nebular gas.

Table 3. Relative atomic abundances used in the impact vaporization model of a differentiated CR chondrite body.

1 Element	2 Bulk composition of CR body[1]	3 CR core[2]	4 CR mantle[2]	5 CR crust[2]	6 Residual CR mantle[2]	7 Residual nebular gas[3]	8 Model plume comp. w/o water[4]	9 Model plume comp. w/ 20% water[5]
H	0.000E+00	0.000E+00	0.000E+00	0.000E+00	0.000E+00	2.790E+10	5.580E+07	5.580E+07
He	0.000E+00	0.000E+00	0.000E+00	0.000E+00	0.000E+00	2.720E+09	5.440E+06	5.140E+06
C	0.000E+00	0.000E+00	0.000E+00	0.000E+00	0.000E+00	6.636E+06	1.327E+04	1.254E+04
N	0.000E+00	0.000E+00	0.000E+00	0.000E+00	0.000E+00	3.122E+06	6.245E+03	5.900E+03
O	3.746E+06	0.000E+00	3.348E+06	3.008E+06	3.444E+06	9.353E+06	3.228E+06	4.769E+06
Na	3.168E+04	0.000E+00	3.171E+04	1.427E+05	5.564E+02	0.000E+00	7.707E+04	7.707E+04
Mg	1.047E+06	0.000E+00	1.048E+06	1.910E+05	1.288E+06	0.000E+00	6.974E+05	6.974E+05
Al	8.230E+04	0.000E+00	8.232E+04	2.801E+05	2.681E+04	0.000E+00	1.632E+05	1.632E+05
Si	1.000E+06	0.000E+00	1.000E+06	1.000E+06	1.000E+06	0.000E+00	1.000E+06	1.000E+06
P	6.882E+03	0.000E+00	7.010E+03	2.567E+04	1.772E+03	3.518E+03	1.464E+04	1.464E+04
S	1.165E+04	1.232E+04	0.000E+00	0.000E+00	0.000E+00	4.341E+05	7.012E+05	6.993E+05
K	1.363E+03	0.000E+00	1.547E+03	7.018E+03	1.063E+01	0.000E+00	3.783E+03	3.783E+03
Ca	5.629E+04	0.000E+00	5.640E+04	1.836E+05	2.067E+04	0.000E+00	1.084E+05	1.084E+05
Ti	4.080E+03	0.000E+00	4.114E+03	1.487E+04	1.094E+03	0.000E+00	8.512E+03	8.512E+03
Cr	1.298E+04	4.807E+03	1.562E+04	1.646E+03	1.969E+04	0.000E+00	2.833E+05	2.825E+05
Mn	5.820E+03	0.000E+00	6.011E+03	2.728E+04	4.132E+01	0.000E+00	1.471E+04	1.471E+04
Fe	9.000E+05	9.000E+05	4.916E+04	1.509E+04	5.872E+04	0.000E+00	5.120E+07	5.107E+07
Co	3.436E+03	3.636E+03	0.000E+00	0.000E+00	0.000E+00	0.000E+00	2.067E+05	2.062E+05
Ni	4.929E+04	5.214E+04	0.000E+00	0.000E+00	0.000E+00	0.000E+00	2.965E+06	2.957E+06
Pd	1.390E+00	1.470E+00	0.000E+00	0.000E+00	0.000E+00	0.000E+00	8.358E+01	8.336E+01
Ir	6.608E-01	6.991E-01	0.000E+00	0.000E+00	0.000E+00	0.000E+00	3.975E+01	3.964E+01

[1]Renazzo composition of Weisberg et al. (1993), modified as in text

[2]See text

[3]See text

[4]94.2 wt% CR core + 1.7 wt% residual CR mantle + 1.7% wt% CR crust + 2.4 wt% of residual nebular gas to yield Ni/H=$3x10^{4}$ and Si/H=500 times their solar values, respectively

[5]93.5 wt% CR core + 1.68 wt% residual CR mantle + 1.68 wt% CR crust + 0.84 wt% water + 2.3 wt% of residual nebular gas to yield Ni/H=$3x10^{4}$ and Si/H=500 times their solar values, respectively